硫化ビスマス超伝導体LaO1-xFxBi1-ySbyS2における不純物効果と超伝導に関する研究

メタデータ	言語: English 出版者: 公開日: 2020-12-15 キーワード (Ja): キーワード (En): 作成者: ワン, イン メールアドレス: 所属:
URL	https://doi.org/10.15118/00010339

Thesis for a Degree of Doctor of Engineering

Study on Superconductivity and Impurity Effects of Bismuth Sulfide Superconductors $LaO_{1-x}F_xBi_{1-y}Sb_yS_2$

硫化ビスマス超伝導体 $LaO_{1-x}F_xBi_{1-y}Sb_yS_2$ における不純物効果と超伝導に関する研究

Wang Ying

Division of Engineering

Course of Advanced Production Systems Engineering

Muroran Institute of Technology

September 2020

Abstract

Recently, significant discoveries have been made in the use of layered materials in novel superconducting (SC) materials. In 2012, superconductivity was discovered in the layered compound $Bi_4O_4S_3$ with SC transition temperature T_c = 8.6 K. Later, $(Eu, Sr)_3F_4Bi_2S_4$ was synthesized under high pressure with T_c = 10 K. Superconductivity was also discovered in $LnO_{1-x}F_xBiS_2$ (Ln = La, Ce, Pr, Nd, Yb) compounds with T_c = 2–10 K through fluorine substitution for oxygen. Further, S can be substituted by Se, and the doped Se preferentially occupies the in-plane S site in $LaO_{1-x}F_xBiCh_2$ (Ch = S, Se) with maximum T_c = 4 K. In particular, the superconductivity of $LaO_{1-x}F_xBiS_2$ compounds has been studied intensively. These compounds have a characteristic structure with an alternate stacking of SC BiS_2 layers and blocking layers (LaO/F) that supply electrons to the BiS_2 layers. The layered crystal structure is analogous to those of high-temperature (high-T_c) cuprate and Fe-based superconductors. However, the mechanism underlying the superconductivity of BiS_2 superconductors, which still remains unclear, is considered to be different from those of cuprate and Fe-based superconductors.

The symmetry of the SC gap is well known to reflect the origin of the SC mechanism. Magnetic penetration depth measurements and thermal conductivity measurements for La- and Nd-based BiS_2 superconductors have shown a full gap with an s-wave. However, transverse-field muon spin relaxation (TF-μSR) measurements have proposed that the SC gap is well described by two-gap s + s-wave model and

anisotropic *s*-wave model. Soon after that, angle-resolved photoemission spectroscopy (ARPES) measurements indicated a large SC gap anisotropy and suggested the existence of accidental nodes in nodal *s*-wave symmetry. Recently, point contact spectroscopy measurements have suggested that the gap symmetry is an unconventional pairing symmetry. Thus, the SC gap symmetry of BiS_2-based superconductors remains controversial.

In this work, we investigated the SC gap symmetry and bulk nature of superconductivity in $LaO_{1-x}F_xBiS_2$ superconductors, and the effect of Sb substitution on the layered superconductor $LaO_{1-x}F_xBi_{1-y}Sb_yS_2$ through XRD, specific heat, electrical resistivity, and magnetic susceptibility measurements. $LaO_{1-x}F_xBiS_2$ (x = 0.5, 0.4) and $LaO_{0.5}F_{0.5}Bi_{1-y}Sb_yS_2$ (y = 0–0.20) were synthesized using the flux method under ambient pressure. $LaO_{1-x}F_xBiS_2$ (x = 0.5, 0.4) show bulk nature of superconductivity, although T_c is slightly suppressed, and its transition is broad for x = 0.4. The electronic specific heat C_e of $LaO_{1-x}F_xBiS_2$ (x = 0.5) below ~ T_c can be explained by *s*-wave superconductivity with either an anisotropic single gap or two gaps. The two-gap effect is more dominant for x = 0.4. The C_e/T at $T<<T_c$ in $LaO_{0.5}F_{0.5}Bi_{1-y}Sb_yS_2$ below y = 0.06 is hardly recovered by Sb substitution, indicating that the superconductivity is robust against the pair-breaking due to non-magnetic impurities, as expected in the fully gapped *s*-wave superconductivity. T_c is suppressed by the Sb-doping in both the specific heat and the electrical resistivity and magnetic susceptibility measurements. The slight decrease in T_c in Sb-doped samples can be ascribed to the enhancement of electron

correlations due to the weak localization of carriers. Based on these experimental results, we conclude that $LaO_{1-x}F_xBiS_2$ compound shows a fully gapped *s*-wave superconductivity.

要 旨

近年、様々な新しい層状超伝導体（SC）が発見され、注目されている。その一つに、2012年に発見された超伝導転移温度$T_c = 8.6$ Kの層状硫化物超伝導体$Bi_4O_4S_3$がある。この系は様々なバリエーションがあり、最も高いT_cをもつ超伝導体は高圧下で合成された10KのT_cを持つ（Eu、Sr）$_3F_4Bi_2S_4$である。また、$LnO_{1-x}F_xBiS_2$（$Ln = $La、Ce、Pr、Nd、Yb）（$T_c = 2$–$10$ K）では、酸素のフッ素置換によりキャリア数を変えることができる。さらに、SをSeに置き換えた$LaO_{1-x}F_xBiCh_2$（Ch＝S、Se）も超伝導を示すことが報告された。ドープされたSeは、$LaO_{1-x}F_xBiCh_2$（Ch＝S、Se）の面内Sサイトを優先的に占有し、最大$T_c = 4$ Kとなる。これらの化合物は、伝導を担うBiS_2層とBiS_2層に電子を供給するブロッキング層（LaO / F）が交互に積層した特徴的な構造を有する。この層状結晶構造は、興味深いことに、高温（高T_c）銅酸化物およびFeベースの超伝導体と類似している。BiS_2超伝導体の超伝導のメカニズムは未だ不明のままであり、銅酸化物やFe系超伝導体とは異なるメカニズムと考えられている。

超伝導発現メカニズムの起源を反映するものとして、超伝導ギャップの対称性がある。LaおよびNdベースのBiS_2超伝導体における磁気侵入長と熱伝導率の測定から超伝導ギャップの対称性として、フルギャップのs波、あるいは、異方的s波とs++波、であることが報告されている。角度分解光電子分光（ARPES）実験からは、超伝導ギャップの大きな異方性が報告され、超伝導ギャップにノードが存在するノーダルギャップの可能性が示唆されている。また、トンネル分光実験からは、超伝導ギャップの対称性がs波のような従来型とは

異なるものであることが報告されている。このように、BiS_2系超伝導体の超伝導ギャップの対称性についてはまだ議論がつづいており、その解明はこの系の超伝導発現メカニズムを解明する上で急務となっている。

BiS_2系超伝導体の中でも、特に$LaO_{1-x}F_xBiS_2$化合物は系統的にキャリア数を変化させることができることから、これまで集中的に研究されてきた。本研究では、$LaO_{1-x}F_xBiS_2$超伝導体の超伝導ギャップ対称性と超伝導性を明らかにする目的で、XRD、比熱、電気抵抗率、磁化率測定を通じて、層状超伝導体$LaO_{1-x}F_xBi_{1-y}Sb_yS_2$に対するSb置換の影響を調べた。$LaO_{1-x}F_xBiS_2$（$x = 0.5$、0.4）および$LaO_{0.5}F_{0.5}Bi_{1-y}Sb_yS_2$（$y = 0$–0.20）の単結晶試料は、大気圧下でフラックス法により作製された。得られた$LaO_{1-x}F_xBiS_2$（$x = 0.5$、0.4）単結晶はどれもバルクの超伝導性を示し、そのT_cは$x = 0.5$で約2.5 K、$x = 0.4$ではわずかに抑制され、約2.4 Kであった。$LaO_{1-x}F_xBiS_2$（$x = 0.5$）の電子比熱C_eは、異方的な単一ギャップまたは 2 ギャップの s 波超伝導によってよく理解できるものであった。$x = 0.4$の場合、特に2ギャップ効果が顕著であった。また、非磁性不純物としてSbを添加した$LaO_{0.5}F_{0.5}Bi_{1-y}Sb_yS_2$では、$T << T_c$での$C_e/T$が少量のSb置換によってほとんど回復しなかった。この結果は$LaO_{1-x}F_xBiS_2$の超伝導がs-波であることを意味する。さらに、比熱の温度依存性、電気抵抗率、磁化率測定から決めたT_cはSbドーピングによって抑制されるが、これはSb不純物による対破壊効果というよりは、キャリアの弱局在によって電子相関が強まったためと考えられる。以上の結果より、$LaO_{1-x}F_xBiS_2$の超伝導はフルギャップのs波超伝導であると結論した。

Contents

Chapter 1

Introduction

Superconductivity is an amazing field of physics and has been attracted so much attention since its discovery in 1911. Today, superconductivity is being applied to many diverse areas such as: theoretical and experimental science, military, transportation, power production, electronics, medicine as well as many other areas. The remarkable phenomenon is famous for zero electrical resistance and Meissner effect. Scientists throughout the world have been striving to understand this remarkable phenomenon for many years.

1.1 A century of superconductivity

Superconductivity was observed for the first time by a Dutch physicist Heike Kamerlingh Onnes, a professor of physics at the University of Leiden. He had first liquefied helium in 1908 below 4.2 K, which gave him the refrigeration technique to reach temperature of a few degrees Kelvin. After 3 years later, he was discovered superconductivity in thin wires of mercury (Hg) by using liquid helium as a low temperature medium. He found the electrical resistivity of Hg abruptly dropped to zero, when the sample was cooled below 4.2 K in 1911. Thus, what he called as superconducting transition temperature T_c. [1] In 1913, he won Nobel Prize in Physics for his research in this field.

After the discovery, the physicists all-around the world were very interested in searching for the possibilities of superconductivity. For decades, a fundamental understanding of this phenomenon included the many scientists who were working in the field. Major breakthroughs came from 1930s and summarized as follows:

- Meissner effect is the expulsion of a magnetic field from a superconductor during its transition from normal state to the superconducting state. German physicists Walther Meissner and Robert Ochsenfeld observed this phenomenon for the first time in 1933. [2]

- London equations are constitutive relations for superconductors and provide simple but useful description of the electrodynamics of superconductivity. These equations were able to explain Meissner effect and developed by brothers Fritz and Heinz London in 1935. [3]

- Ginzburg-Landau theory is a mathematical physical theory used to describe superconductivity based on general symmetry properties. It named after Vitaly Lazarevich Ginzburg and Lev Landau in 1950. [4]

- BCS theory is the first microscopic mechanism of superconductivity and explains the superconducting phenomena by a condensation of paired electrons called Cooper pairs. It put forward by Bardeen, Cooper and Schrieffer in 1957. [5-6]

- Josephson effect which was a mathematical prediction of relations between current and voltage across a weak link. It predicted by British physicist Brian David Josephson in 1962. [7]

- Discovery of a barium-doped lanthanum copper oxide ($La_{2-x}Ba_xCuO_4$) superconductivity by J Georg Bednorz and K Alex Műller in 1986 [8] with $T_c = 35$ K, which led to a new flood of high temperature superconductors. After few years, Wu and Chu found a maximum $T_c \sim 93$ K from YBaCuO [9] and later Maeda group discovered first 100 K superconducting transition temperature in BiSrCaCuO [10] compound.

- ➢ Discovery of superconductivity in MgB_2 by Akimitsu group in 2001 [11] with T_c more than 30 K.

- ➢ Discovery of iron-based superconductors LaFePO layer compound by Kamihara group in 2006 [12] with $T_c = 4$ K. Since after, the maximum attained $T_c = 26$ K in 2008 [13] has been observed from $LaO_{1-x}F_xFeAs$ compound by the same group.

- ➢ Discovery of BiS_2-based superconductors by Mizuguchi group in 2012 [14] with $T_c = 6$ K. We will illustrate the BiS_2-based superconductors in detail in 1.5 part.

1.2 Significant phenomena and theories of superconductors

1.2.1 Zero electrical resistivity

Superconductivity manifests itself mainly as an absence of resistivity below some superconducting transition temperature T_c. It is one of two fundamentally important and intuitively startling properties are associated with superconductivity. The state of matter in which electrical resistivity is zero is known as the “superconducting state” as shown in Fig. 1.1(a). As is well-known, a superconductor is an element or metallic alloy, which when cooled to near absolute zero, dramatically lose all its electrical resistance. In principle, superconductors can allow electrical current to flow without any energy loss called perfect conductivity.

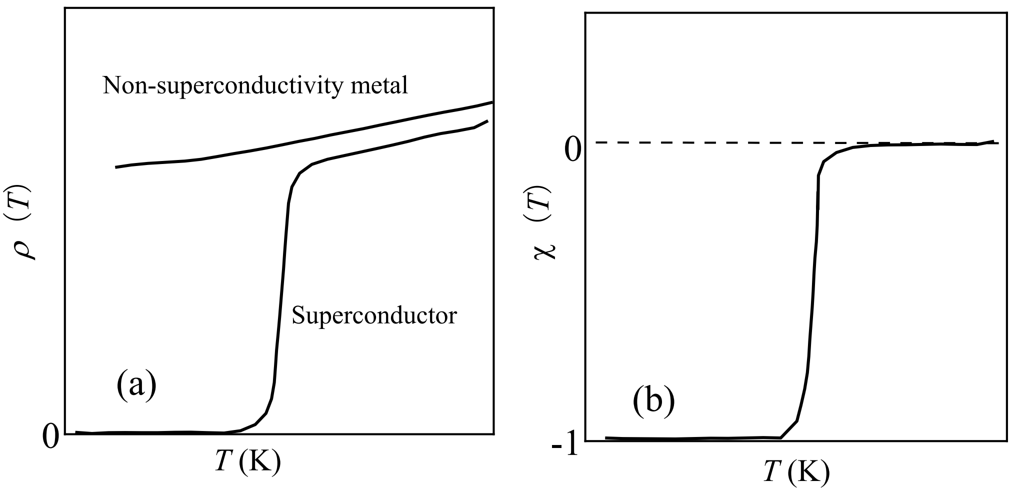

Fig. 1.1 Basic phenomenon of superconductors: (a) zero electrical resistance, and (b) Meissner effect.

1.2.2 Meissner effect

The next fundamental property of superconductivity is perfect diamagnetism called Meissner effect found in 1933. When a superconductor is cooled below its transition temperature in a magnetic field, it excludes the magnetic flux. In other words, the material becomes fully diamagnetic in the superconducting state as shown in Fig. 1.1(b). The expulsion of magnetic field in a superconductor at room temperature and below T_c is shown in Fig. 1.2.

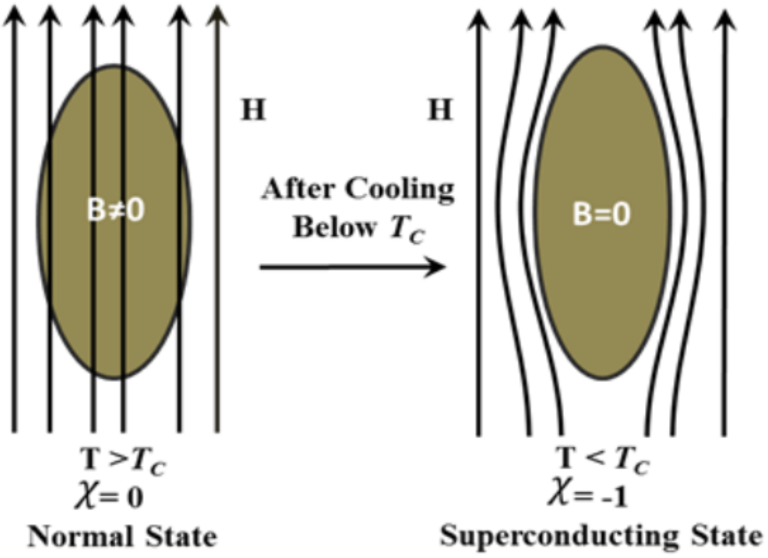

Fig. 1.2 Meissner effect in a superconducting in a constant applied magnetic field.

1.2.3 Critical parameters of superconductors

The superconducting state of a material is decided by three parameters such as temperature, magnetic field and electrical current. That three parameters called critical temperature (T_c), critical magnetic field (H_c), and critical current density (J_c) respectively. T_c is the temperature below which the material becomes a superconductor. H_c is the maximum magnetic field which can be held out by a material in the superconducting state and J_c is the maximum current that can be tolerated by a superconductor in the superconducting state. These three parameters are coupled together to define the superconducting limits of a material as shown in Fig. 1.3 which shows that for the occurrence of superconductivity in a material. The phase diagram between these three parameters for a material gives a surface called as critical surface, beneath the surface the material is in superconducting state and above the surface the material is in normal state.

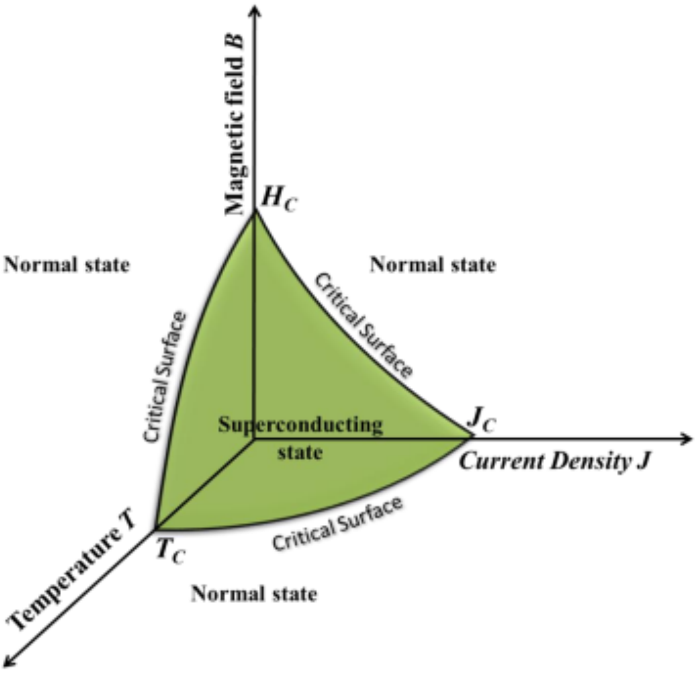

Fig. 1.3 Schematic phase diagram of critical surface for a superconductor.

1.2.4 The London equations

In 1935, Fritz and Heinz London theoretically explained the Meissner effect by postulating two groups of electrons in a superconducting material, the superconducting electrons and the normal state electrons. They employed the Maxwell's equations to develop a set of electrodynamics equations, called the London equations. The description is shown as follow:

$$\frac{\partial \boldsymbol{J}_s}{\partial t} = \frac{n_s e^2}{m}\boldsymbol{E}$$

$$\nabla \times \boldsymbol{J}_s = -\frac{n_s e^2}{m}\boldsymbol{B}$$

Where J_s is the superconducting current density, E and B are the electric and magnetic field within superconductor respectively, e is the charge of an electron, m is electron mass, and n_s is a constant associated with a number density of superconducting carriers.

According to the London equations, the magnetic field exponentially falls off with increasing distance from the surface of a superconducting sample. This characteristic decay length is called the London penetration depth ($\lambda = \sqrt{\frac{m}{n_s e^2 \mu_0}}$): typical values are from 50 to 500 nm.

1.2.5 The Ginzburg-Landau (GL) theory

In 1950, V. Ginzburg and L. Landau developed a theoretical explanation for superconductors based on general symmetry properties. This theory was put forward before BCS theory, but it is crucial for next research. The GL theory introduces a characteristic length, now usually called the GL coherence length ($\xi = \sqrt{\frac{\hbar^2}{2m|\alpha|}}$), which α is an expansion coefficient in a phenomenological model. The ratio of the two characteristic lengths defines the GL parameter:

$$\kappa = \frac{\lambda}{\xi}$$

For type I superconductors, $0 < \kappa < 1/\sqrt{2}$.

For type II superconductors, $\kappa > 1/\sqrt{2}$.

1.2.6 The BCS theory

The next step in the evolution of our understanding of superconductors was the establishment of the existence of an energy gap Δ, of order $k_B T_c$ between the ground state and the quasi-particle excitation of the system. In 1957, three American Physicists-John Bardeen, Leon Cooper and John Schrieffer produced their epoch-making pairing theory of superconductivity, known as the BCS theory. The BCS theory explains that even a very weak attractive interaction between electrons, mediated by phonons, creates a bound pair of electrons, called the Cooper pair, occupying states with equal and opposite momentum and spin. The formation of the bound states creates instability in the ground state of the Fermi sea of electrons and a gap $\Delta(T)$ opens at the Fermi level. The minimum energy $E_g = 2\Delta(T)$ should be required to break a Cooper pair, creating two quasi-particle excitations. This $\Delta(T)$ was predicted to increase from zero at T_c to a limiting value

$$E_{\mathrm{g}} = 2\Delta(0) = 3.528 k_{\mathrm{B}} T_{\mathrm{c}}$$

For $T \ll T_c$. This prediction provided one of the most decisively early verification of microscopic theory.

The energy gap can be evaluation based on BCS theory in the weak-coupling limit $N(0)V \ll 1$, as follow:

$$\Delta = 2\hbar\omega_{\mathrm{D}} e^{-\frac{1}{N(0)V}}$$

where $N(0)$ is the electronic density of states at the Fermi level and V is the attractive electron-phonon coupling potential and $\hbar\omega_D = k_B\Theta_D$ is Debye cutoff energy. The superconducting transition temperature T_c is the temperature at which $\Delta(T) \rightarrow 0$. In this case:

$$T_{\mathrm{c}} = 1.13\Theta_{\mathrm{D}} e^{-\frac{1}{N(0)V}}$$

T_c is in part determined by the Debye temperature so that an observable shift in Θ_D should accompany an alteration of T_c. Comparing this with energy, we can see that:

$$\frac{\Delta(0)}{k_B T_c} = \frac{2}{1.13} = 1.764$$

So that the gap at $T = 0$ is indeed comparable in energy to $k_B T_c$. The numerical factor 1.76 provided the number of the 2Δ(0) above. The factor has been tested in many experiments and found to be reasonable.

For weak-coupling superconductors, the reduced gap $\Delta(T)/\Delta(0)$ is a universal function of the reduced temperature T/T_c, which decreases monotonically from 1 at $T = 0$ to zero at T_c, as shown in Fig. 1.4. Near $T = 0$, the temperature variation is exponentially slow since $e^{-\Delta/k_B T} \approx 0$, so that $\Delta(T) \approx \Delta(0)$ is nearly constant until a significant number of quasi-particles are thermally excited. Near the critical temperature T_c, the relation asymptotes to:

$$\frac{\Delta(T)}{\Delta(0)} \approx 1.74(1 - \frac{T}{T_c})^{1/2}$$

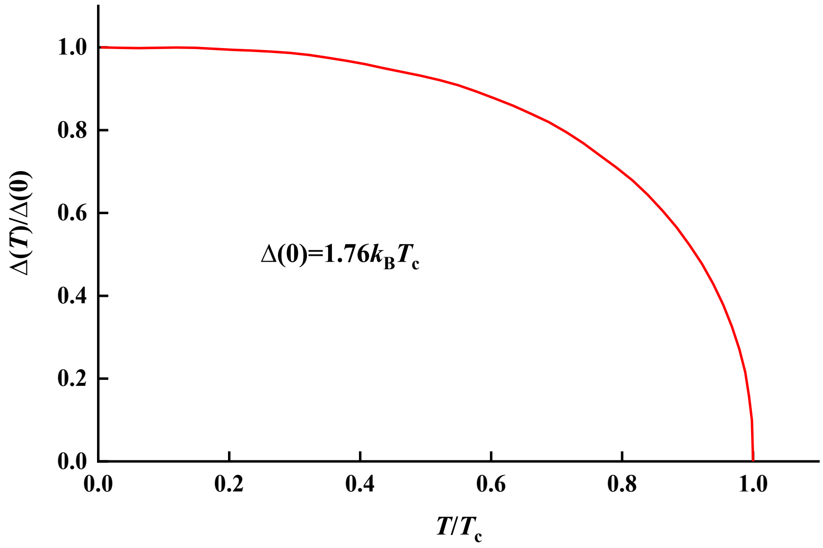

Fig. 1.4 Variation of T/T_c with $\Delta(T)/\Delta(0)$ according to the BCS theory.

As a successful superconducting theory, BCS theory can explain the basic phenomenon of superconductivity with a unified microscopic mechanism, such as specific heat:

$$C_{\mathrm{es}} = T\frac{dS}{dT} = 2\beta k_{\mathrm{B}} \sum_{k} \left(-\frac{\partial f_k}{\partial E_k}\right)\left(E_k^2 + \frac{1}{2}\beta\frac{d\Delta^2}{d\beta}\right)$$

The first term is the usual one coming from the redistribution of quasi-particles among the various energy states as the temperature changes. The second term is more unusual and describes the effect of the temperature-dependent gap in changing the energy levels themselves. Near $T = T_c$, as $\Delta(T) \to 0$, the first term then reduces to the usual normal-state electronic specific heat:

$$C_{\mathrm{en}} = \gamma T = \frac{2}{3}\pi^2 k_{\mathrm{B}}^2 N(0)T$$

The jump of electronic specific heat ΔC at T_c is evaluated as $C_{\mathrm{es}} - C_{\mathrm{en}}$, as follows:

$$\Delta C = 9.4N(0)k_{\mathrm{B}}^2 T_{\mathrm{c}}$$

Comparing this with C_{en}, the normalized magnitude of the discontinuity is:

$$\frac{\Delta C}{C_{\mathrm{en}}} = \frac{9.4}{2\pi^2/3} = 1.43$$

For weak-coupling superconductor, it basically goes well with experiment value.

1.2.7 The Josephson effect

A Josephson junction is made by sandwiching a thin layer of non-superconducting material between two layers of superconducting material, which consists of two or more superconductors coupled by a weak link. The weak link can consist of a thin insulating barrier (known as a superconductor–insulator–superconductor junction, or S-I-S), a short section of non-superconducting metal (S-N-S). The devices are named after Brian Josephson, who predicted in 1962 that pairs of superconducting electrons could “tunnel” right through the non-superconducting barrier from one superconductor to another, which is known as Josephson effect or Superconducting tunneling effect. He also predicted the exact form of the current and voltage relations for the junction of superconducting–non-superconducting–superconducting layers across the weak link. An experimental work proved that he was right, and hence Josephson was awarded the 1973 Nobel Prize in physics for this work.

1.2.8 Classification of superconductors

Superconducting materials can be categorized in various ways which is schematically represented in Fig. 1.5. The classifications of superconductors are mainly based on their critical temperature, behavior in an applied field and the superconducting mechanism.

Based on critical temperature, superconductors are classified into high temperature superconductors (HTS) if it has a $T_c > 77$ K and low temperature superconductors (LTS) if it has a $T_c < 77$ K. But this classification is not rigid, many other materials with T_c higher than 30 K also belong to HTS group such as MgB_2 and iron-based superconductors.

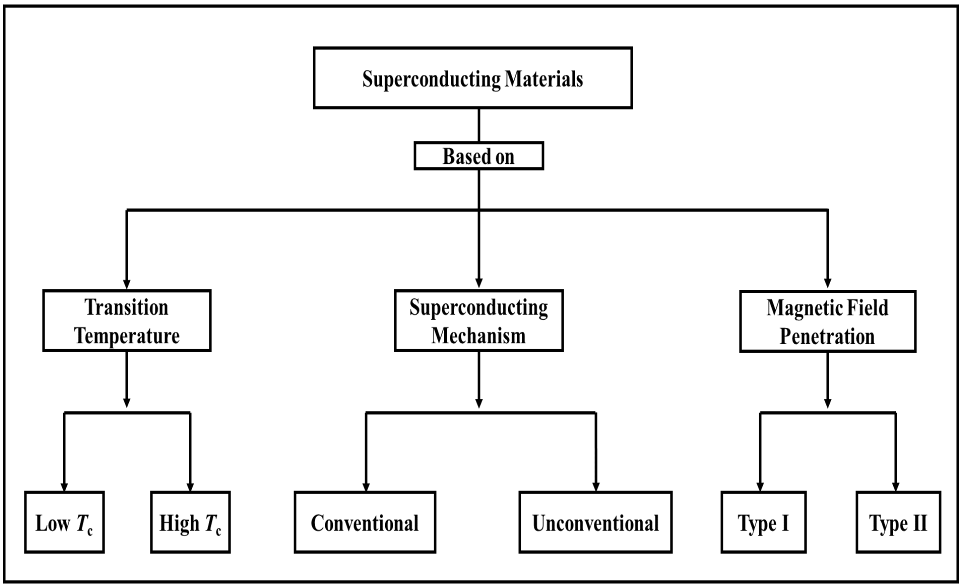

Fig. 1.5 Schematic representation of the superconductor classification.

Based on superconducting mechanism superconductors are classified as conventional superconductors and unconventional superconductors. Superconductors which fit into the BCS framework are known as conventional superconductors. Superconductors whose behavior cannot be explained by BCS theory are known as unconventional superconductors. Formation of Cooper pairs by electron-phonon interaction is depicted in the Fig. 1.6. The Cooper pair state is responsible for superconductivity. When an electron moves in a crystal lattice, it will attract positive charges on the adjacent lattice points, causing local distortion of the lattice points, forming a localized region with high positive charges. This local region of high positive charge will attract electrons with opposite spins and pair with the original electrons with a certain binding energy. At very low temperatures, this binding energy may be higher than the energy of the lattice atom vibration. In this way, the Copper pair will not exchange energy with the lattice, and there is no resistance, forming the so-called "superconductivity".

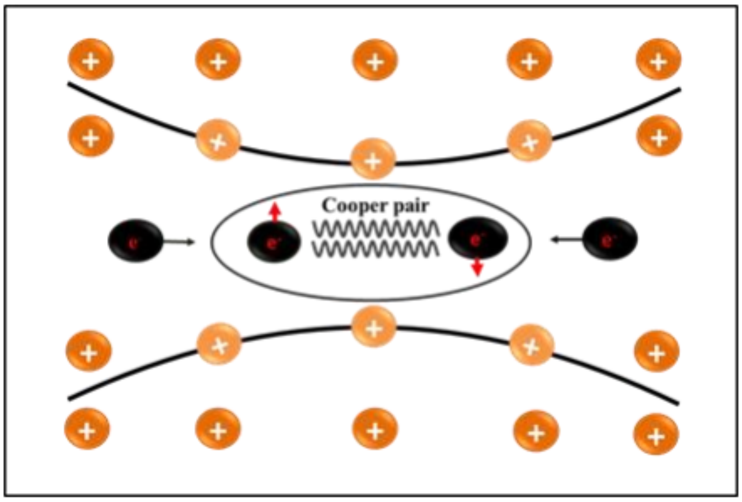

Fig. 1.6 Formation of Cooper pair in a superconducting material- BCS mechanism.

Based on the behavior of a superconductor in an external magnetic field, superconductors are classified into two categories type I and type II superconductors as shown in Fig. 1.7. For type I superconductors, its superconducting properties will be lost at moment. Type I superconductors expel the external magnetic field from its core up to a critical field (H_c). For external fields above H_c, the superconductor becomes normal material. For type II superconductors, it has superconducting electrical properties up to a field denoted by H_{c2}. Between the lower critical field H_{c1} and the upper critical field H_{c2} the Meissner effect is incomplete, and this region called as mixed state.

An important difference between type I and type II superconductors is the mean free path of the conduction electrons in the normal state. If the coherence length ξ is longer than the penetration depth λ, the superconductor will be type I, with $\kappa < 1/\sqrt{2}$; $\kappa = \lambda/\xi$. But when the mean free path is short, the coherence length ξ is short and the penetration depth λ is great with $\kappa > 1/\sqrt{2}$, and the superconductor will be type II. Type I superconductors are conventional superconductors and they are well described by the BCS theory.

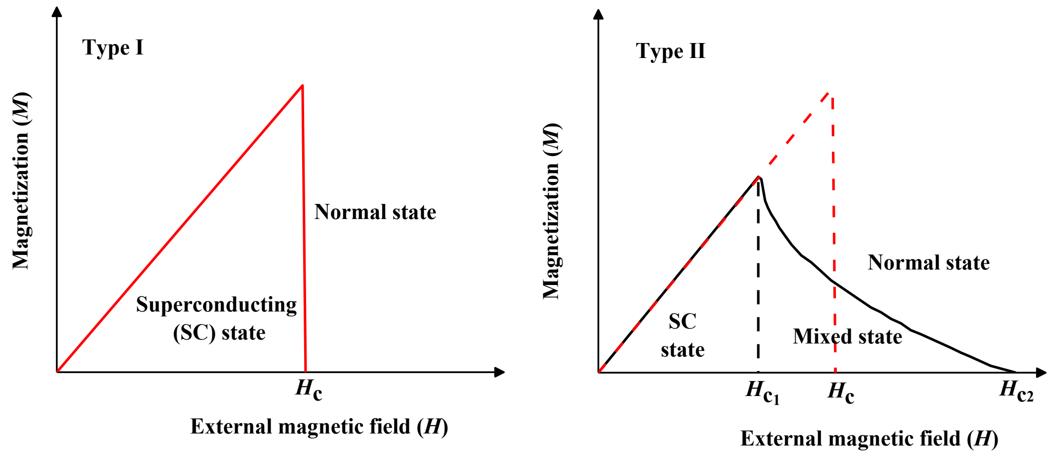

Fig. 1.7 Magnetization versus external magnetic field for type I and type II superconductors.

1.3 Superconducting materials and applications

1.3.1 Superconducting materials

Ever since the invention of superconductivity in 1911, researchers around the world tried to raise the superconducting transition temperature by different methods under different conditions. Even though there are thousands of superconductors known today, only a very small number of them are used for practical applications. The first element to display superconductivity is Hg following which many materials including metals, compounds, cuprates, iron-based and chalcogenides et.al turned out to be superconductors at critical temperatures ranging from a few kelvins to 164 K under different conditions. Some of superconducting materials are listed in Table 1.1. [15-35]

Table 1.1 List of some superconducting materials.

Type	Example	T_c (K)
Elements	Al	1.2
	In	3.4
	Sn	3.7
	Pb	7.2
	Nb	9.3
	α-Hg	4.2
	α-La	4.9
	Ta	4.5
Compounds	MgB_2 [11]	30
	Nb_3Ge [15]	23.2
	V_3Ga [16]	16.5
	Nb_3Sn [17]	18.05
	V_3Si [18]	17
Cuprates	$La_{1.85}Ba_{0.15}CuO_4$ [8]	35

	$YBa_2Cu_3O_7$ [9]	93
	$Bi_2Sr_2Ca_2Cu_3O_{10}$ [10]	100
	$HgBa_2CuO_4$ [19]	94
	$HgBa_2Ca_2Cu_3O_8$ [20]	135
	$Tl_2Ba_2Ca_2Cu_3O_{10}$ [21]	125
Iron-based	LaFeAs(O, F) [13]	26
	CeFeAs(O, H) [22]	48
	SmFeAs(O, F) [23]	55
	FeSe [24]	65
	Na(Fe, Co)As [25]	20
Chalcogenides	$AuTe_2$ [26]	2.3
	(Ir, Rh)Se_2 [27]	10
	(Ir, Pt)Te_2 [28]	3.1
BiS_2-based layered	$Bi_4O_4S_3$ [14]	6
	La(O, F)BiS_2 [29]	10.6
	(La, Sm)(O, F)BiS_2 [30]	10.3
	Yb(O, F)BiS_2 [31]	5
	Nd(O, F)BiS_2 [32]	6.4
	Ce(O, F)BiS_2 [33]	6.7
	Pr(O, F)BiS_2 [34]	8.7
	La(O, F)$BiSe_2$ [35]	6.7

1.3.2 Application of superconductors

Soon after Kamerlingh Onnes discovered superconductivity, scientists began dreaming up practical applications for this strange phenomenon. The two properties of superconductors, zero resistivity and perfect diamagnetism, can be used to enhance the performance of many devices. In general, applications of superconductor can be divided into small scale and large scale categories. Small scale applications include Josephson devices, Superconducting Quantum Interference Devices (SQUID), microwave devices and resonators. Large scale applications include electric power transmission, superconducting magnets, magnetic resonance imaging (MRI), energy storage devices, magnetic levitation devices, magnetic confinement in fusion reactors and particle accelerators. Small scale applications are expected to be commercialized earlier than large scale applications due to the complexity in fabricating these materials suitable for commercial applications. Cooling superconductors much below room temperature is the main hurdle which restricts their use in day to day life. A superconductor which can be operated at a temperature close to room temperature is a dream of any one in this research area because of its potential to change the world.

1.4 Brief introduction of cuprates and iron-based superconductors

1.4.1 Brief introduction of cuprates

Since the discovery of high temperature superconductivity in $La_{2-x}Ba_xCuO_4$, the following few years saw a surge of novel superconductors with related crystal structure. They are collectively called ‘cuprates’, because they share a common structural and functional unit, a layer constituted of Cu and O atoms. The schematic image of the crystal structure of cuprates $Bi_2Sr_2CuCa_2O_8$ (Bi2212) is shown in Fig. 1.8. The Cu-O surface of the conductive layer where superconductivity is developed and the blocking layer that supplies carriers to the conductive layer have a layered structure in which the volume is increased in the *c*-axis direction. Another point to note in the crystal structure is that the Cu-O plane, which is the superconducting layer, forms a two-dimensional square lattice with CuO_2 as a unit. The T_c of the cuprates exceeded those known at the time by an order of magnitude. The physical properties of cuprates were studied with increased sensitivity over time. However, it quickly became clear that much of the theory used to explaining the electric and magnetic properties of cuprates and unconventional *d*-wave paring with strongly correlated electron system was identified, instead of conventional *s*-wave paring.

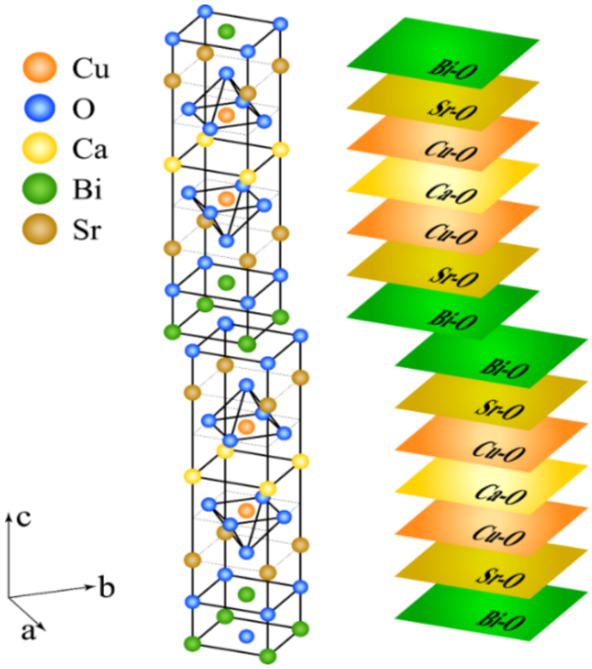

Fig. 1.8 The crystal structure of cuprates $Bi_2Sr_2CuCa_2O_8$ (Bi2212).

The superconductivity in cuprates depends heavily on temperature and doping concentration. Shown in Fig. 1.9 is the schematic phase diagram of hole doped cuprates. The horizontal axis denotes the doping level controlling the electron concentration in the Cu-O planes. The parent compound in which carriers are not doped, it becomes a Mott insulator due to the repulsion of two electrons on the same atom and exhibits anti-ferromagnetism. Superconductivity develops when holes are doped, but on the underdoped side is mysterious pseudogap characterized by T^*at temperatures above T_c. In the superconducting state, an energy gap called a superconducting gap opens on the Fermi surface and many studies have revealed that the symmetry of this gap is *d*-wave symmetry. The mechanism of superconductivity in cuprates has not been fully clear, and elucidation of the mechanism is an important issue in physics. At present, it is thought that unique properties such as pseudogap and charge order are the key to elucidating the mechanism of superconductivity.

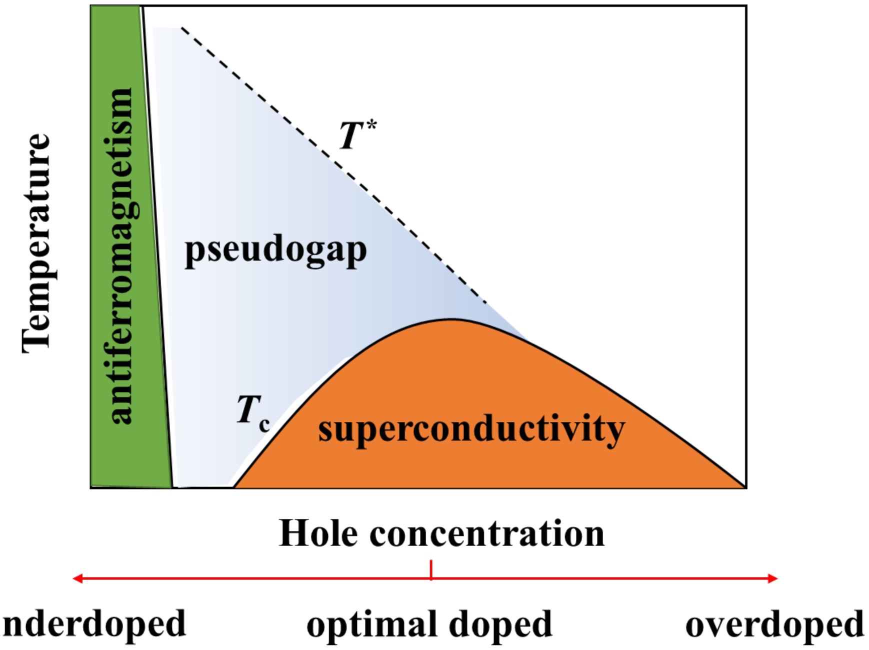

Fig. 1.9 The schematic phase diagram of hole doped cuprates.

1.4.2 Brief introduction of iron-based superconductors

For over twenty years cuprates stood as the sole class of high T_c superconductors, until the advent of iron pnictide material $LaFeAsO_{1-x}F_x$. Iron-based superconductors have the highest T_c next to cuprates, and quickly attracted so much attention at that time. Iron-based superconductors have attracted attention because of their high T_c and the fact that the superconducting layer contains iron, which is considered incompatible with superconductivity because of its magnetic properties. As for the crystal structure is shown in Fig. 1.10, $LaO_{1-x}F_xFeAs$ superconductor also has a layered structure in which the superconducting layer (Fe-As) and the blocking layer (La-O/F) have a volume in the *c*-axis direction like cuprates. The Fe-As layer has a structure in which iron atoms are tetrahedral coordinated with arsenic atoms and is characterized by forming a two-dimensional square lattice like cuprates. However, iron-based superconductors are different from cuprates, and the constituent elements of the superconducting layer may be different. Such as the superconducting layers will be Fe-P in the $LnO_{1-x}F_xFeP$ (Ln = La, Ce, Pr, Nd, Sm) superconductors. $LaO_{1-x}F_xFeAs$ superconductor supplies a carrier by partial defect of the O site of the blocking layer or fluorine substitution of the O site, and superconductivity is developed. The parent compound exhibits anti-ferromagnetism in a low temperature region and does not have a superconducting transition. In many iron-based superconductors other than $LaO_{1-x}F_xFeAs$, the possibility of unconventional superconductivity due to antiferromagnetic fluctuations has been pointed out. Although the gap symmetry of some iron-based superconductors also proposed to be *s*-wave, so far there is not common understanding.

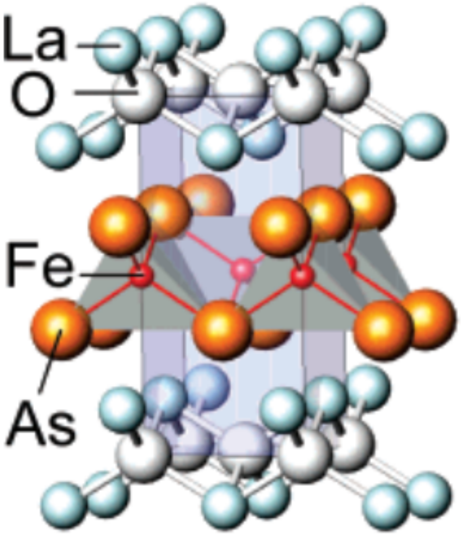

Fig. 1.10 The crystal structure of $LaO_{1-x}F_xFeAs$.

1.5 Introduction of BiS_2-based superconductors

1.5.1 The crystal structure of BiS_2-based superconductors

In 2012, layered superconductors $Bi_4O_4S_3$ with a BiS_2-type superconducting layer were discovered by by Mizuguchi group. [14] Because the similar crystal structure with cuprates and iron-based superconductors, it become the popular topic quickly. The common crystal structure in these superconductors is an alternate stacking of the superconducting (SC) layer and blocking (BL) layers by forming a two-dimensional square lattice in the *c*-axis direction. The crystal structure of the $Bi_4O_4S_3$ superconductor is composed of alternate stacks of the BiS_2 SC layer (Bi_2S_4 bilayer) and the $Bi_4O_4(SO_4)_{0.5}$ BL layer as shown in Fig. 1.11. By replacing the BL layer by a simple REO layer (RE: rare earth), $REO_{1-x}F_xBiS_2$ superconductors were discovered as shown in Fig. 1.12. [29-34]

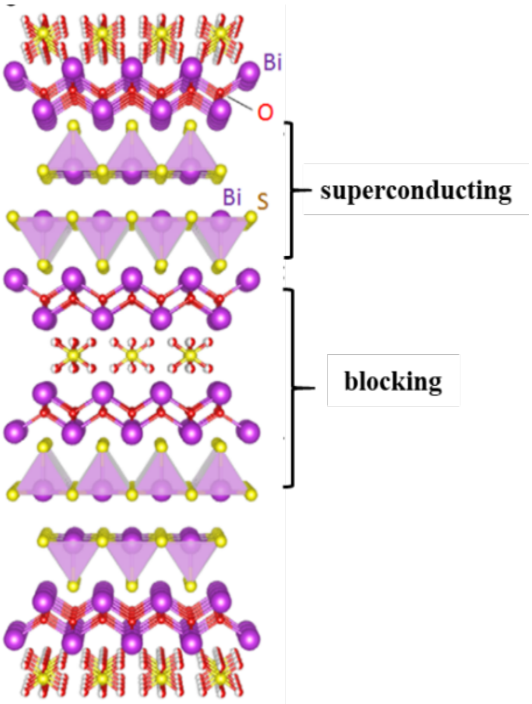

Fig. 1.11 The crystal structure of $Bi_4O_4S_3$.

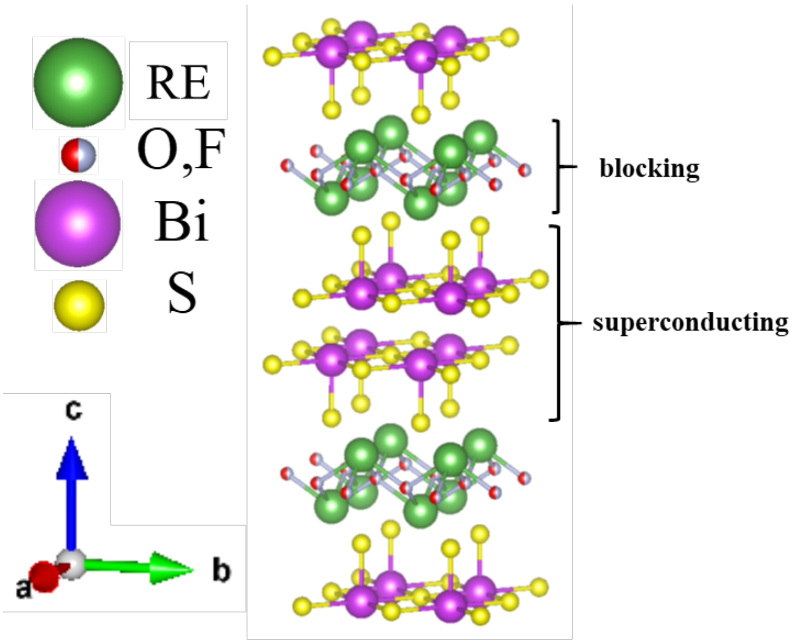

Fig. 1.12 The crystal structure of $REO_{1-x}F_xBiS_2$.

Band calculation suggested that the conduction band of BiS_2-based superconductors are mainly composed of Bi $6p_x$ and $6p_y$ orbitals hybridized with S 3p orbitals; so that, the BiS_2 layer acts as a SC layer in the BiS_2-based superconductors. The space group of $Bi_4O_4S_3$ compound is tetragonal $I4/mmm$ and almost all $REOBiS_2$ compounds are tetragonal $P4/nmm$. For $Bi_4O_4S_3$ superconductor, the electron carriers are generated by the SO_4 defects: the valence states can be described as $(Bi^{3+}{}_2O^{2-}{}_2)_2(SO_4{}^{2-})_{0.5}(Bi^{3+}S^{2-}{}_2)_2 \bullet e^-$, where e^- denotes a doped electron. Among the BiS_2-based superconductors, the $REOBiS_2$-based phases have been mostly studied owing to their simple structure to grow and easy carrier doping control. The first report on the superconductivity in the $REOBiS_2$-based superconductor was $LaO_{1-x}F_xBiS_2$. The parent phase ($x = 0$) is a band insulator. F substitution is effective to make the phase metallic, and superconductivity is observed in the doped phases. Electron doping in $LaOBiS_2$ can be achieved by F^- substitution for the O^{2-} site or cation substitution (cation with a valence higher than 3+, such as Ti^{4+}) for the La^{3+} site. In addition, various of $REOBiS_2$-based superconductors can be synthesized by replacing La by Ce, Pr, Nd, Sm, or Yb. [29-34] Also, the S site can be substituted by selenium and the doped Se tends to occupy the in-plane site in $LaO_{1-x}F_xBiCh_2$(Ch: S, Se). [35-36] Because of the presence of a van der Waals gap between the BiS planes, the plate-like single-crystal can be easily exfoliated in $REOBiS_2$-based superconductors. The transport measurements with single-crystal revealed a huge anisotropy of electronic conductivity and superconductivity (H_{c2}) in the BiS_2-based compounds.

1.5.2 The pressure effect of BiS_2-based superconductors

When pressure is applied to a substance, its crystal structure or electronic state changes, which may affect physical properties. BiS_2-based superconductors are pressure-sensitive superconductors, such as external pressure and chemical pressure, and it is known that T_c greatly changes with pressure.

The temperature dependence of electrical resistance and XRD patterns are shown in Fig. 1.13 and Fig. 1.14 by Mizuguchi group, [29, 37] T_c markedly increases in $LaO_{0.5}F_{0.5}BiS_2$ by annealing the as-grown crystal under high pressure (HP). The shielding volume fraction (superconducting phase) also markedly enhanced by HP annealing from magnetic susceptibility measurement by the same group. This change in superconductivity is related to the introduction of strain in the grains. The X-ray diffraction peaks are broadened after HP processing. There is a pressure-induced structure phase transition from tetragonal to monoclinic. Basically, BiS_2-based compounds possess a structural instability, [38] probably due to the presence of lone-pair electrons of Bi. [39] From the pair distribution function (PDF) analysis, the intrinsic nature of in-plane structural fluctuations and the possibility of charge fluctuations linked to the superconductivity were proposed. [40] Furthermore, the $LaO_{0.5}F_{0.5}BiS_2$ sample prepared by single-step HP synthesis showed the highest T_c of 11.5 K among the BiS_2-based compounds. [41]

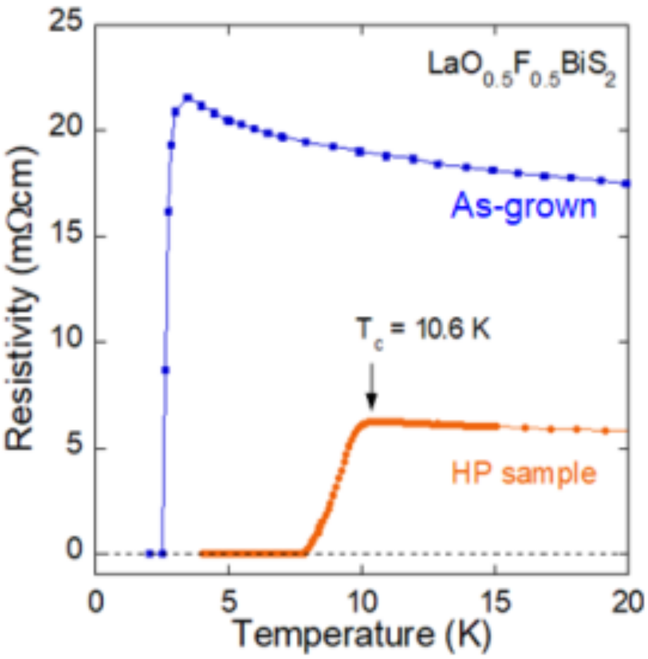

Fig. 1.13 Temperature dependences of electrical resistivity for as-grown and HP-annealed samples of $LaO_{0.5}F_{0.5}BiS_2$.

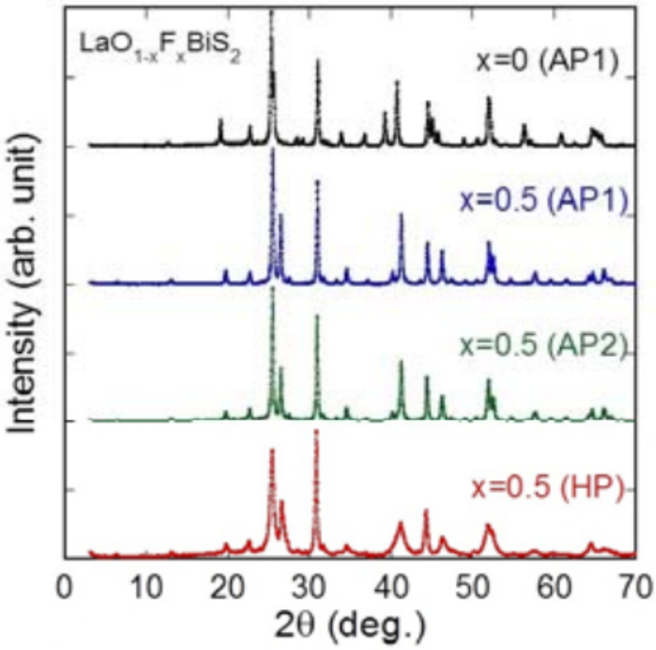

Fig. 1.14 X-ray diffraction patterns for as-grown and HP-annealed samples of $LaO_{0.5}F_{0.5}BiS_2$.

For $REOBiCh_2$ system superconductors, T_c also increases due to the chemical pressure (CP) effect accompanying elemental substitution. Using the CP effect, we can obtain effects like those obtained using the HP technique. There are two typical CP effects for these superconductors: one is the RE-site substitution with RE^{3+} that the ionic radius smaller than La^{3+}, the other is the in-plane S site substitution with Se^{2-} that the ionic radius larger than S^{2-} as shown in Fig. 1.15. The CP can be induced by lattice shrinkage and expansion respectively in both two ways, and T_c increases with increasing in-plane CP. [42] In order to compare the magnitude of in-plane CP, the equation CP = $(R_{Bi}+R_{Ch1})$/(Bi-Ch1(in-plane) distance) was proposed by Mizuguchi group, where R_{Bi} and R_{Ch1} are the ionic radius of Bi and Ch in the Bi-Ch1 plane as shown in Fig. 1.16. It has been confirmed that the superconductivity of this system is affected by the crystal structure, but the relationship between the crystal structure and superconductivity is not clear yet, although the in-plane Bi-Ch bond distance and the Ch-Bi-Ch bond angle are important.

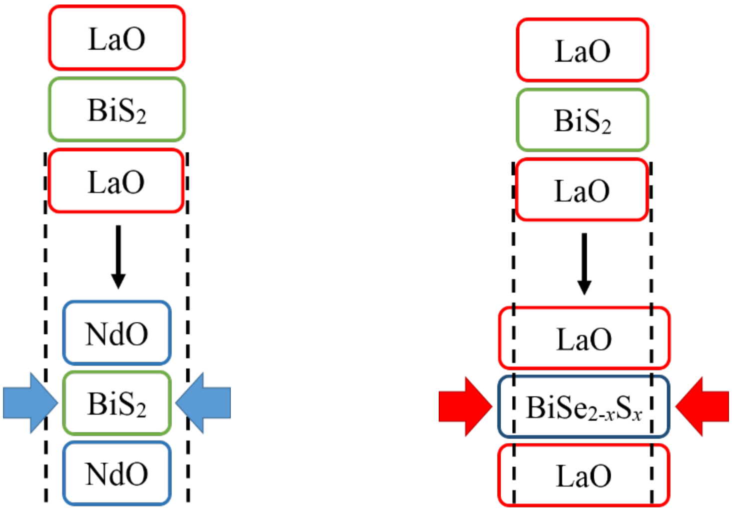

Fig. 1.15 Schematic image of in-plane CP effect in $REO_{0.5}F_{0.5}BiS_2$ and $LaO_{0.5}F_{0.5}BiS_{2-x}Se_x$.

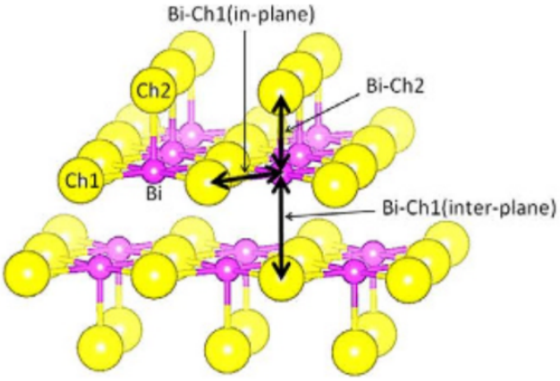

Fig. 1.16 Schematic image of the Bi, Ch1 and Ch2 sites, and three Bi-Ch distances: Bi-Ch1 (in-plane), Bi-Ch1(inter-plane), and Bi-Ch2.

1.5.3 Bulk superconductivity and filamentary superconductivity of $LaO_{0.5}F_{0.5}BiS_2$

If the superconducting phase volume fraction of materials is lump, it will be bulk superconductors, otherwise will be filamentary superconductors. In the case of a superconducting material, a melt-grown material obtained by melting and then growing crystals is referred to as a bulk. The superconducting bulk has properties like those of a permanent magnet and has a stronger magnetic force than a permanent magnet. Therefore, a wide range of application is considered. As 1.5.2 part has mentioned, the superconductivity of $LaO_{0.5}F_{0.5}BiS_2$ has proposed as filamentary under ambient pressure, and as bulk under HP technique. [29, 43] Similarly, the superconductivity is bulk in nature from both the two typical CP effects. The number of in-plane CP ~ 1.011 is estimated boundary of bulk superconductivity and non-superconductivity. [42] As described above, it has been reported that $LaO_{0.5}F_{0.5}BiS_2$ has a filamentary superconductivity from the discussion of the absolute value of Meissner diamagnetism and the in-plane chemical pressure. However, the jump of specific heat accompanying the superconducting transition was observed by Yazici group [31] from the specific heat measurement of $LaO_{0.5}F_{0.5}BiS_2$ polycrystal as shown in Fig. 1.17. Specific heat measurement is one of the most powerful means of examining the bulk properties of superconductivity compared to Meissner diamagnetism. Thus, from this result, $LaO_{0.5}F_{0.5}BiS_2$ has the potential to essentially become bulk superconductivity. Whether the observed superconductivity is bulk or occurred in surface, it is crucial to elucidate the mechanism of superconductivity.

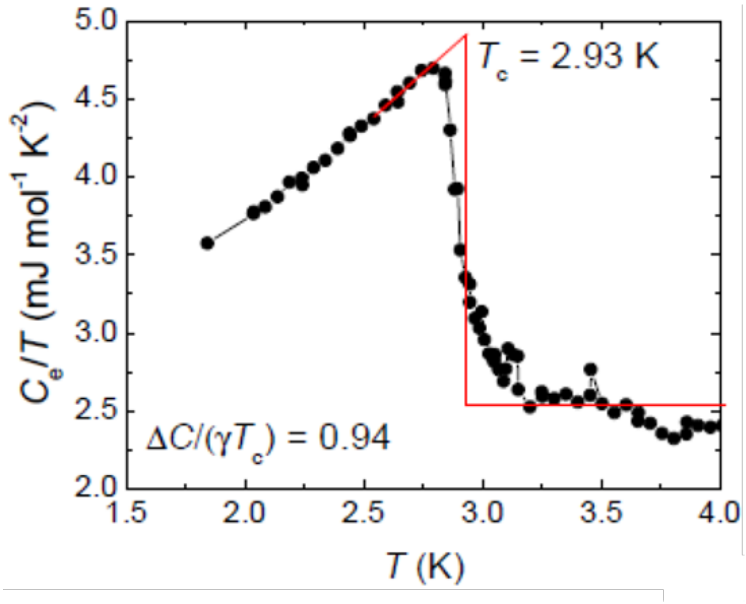

Fig. 1.17 The plot of electronic specific heat C_e divide T versus temperature.

1.5.4 The superconducting gap symmetry of BiS_2-based superconductors

The superconducting gap can be defined as the energy difference between the ground state of the superconductor and the energy of the lowest quasiparticle excitation. As is well known, the symmetry of the superconducting gap reflects the origin of the superconducting mechanism. According the results already reported in literature, we consider the possibility of three types as shown in Fig. 1.18. [44] The first one is the conventional *s*-wave with energy gap Δ isotropic in ***k***-space; $\Delta(\boldsymbol{k}) = \Delta_0$, also means the superconducting gap has no dependence in ***k***-space that so called a full gap. The second one is the unconventional *d*-wave with energy gap Δ has nodes and anti-nodes dependence of ***k***-space; $\Delta(\boldsymbol{k}) = \Delta_0 (\cos k_x - \cos k_y)$, such as cuprate superconductors. The third one is the conventional *s*-wave with energy gap Δ anisotropic in ***k***-space; $\Delta(\boldsymbol{k}) = \Delta_0 + \Delta_2 (\cos k_x - \cos k_y)^4$, also means the superconducting gap has large gap and small gap dependence of ***k***-space. In unconventional superconductivity, nodes do not always exist, such as the superconducting gap of iron-based superconductors, which is considered as unconventional superconductivity, has been proposed as $s\pm$ wave with full gap. Strictly speaking, even in conventional superconductivity, the superconducting gap is not completely isotropic due to the symmetry of the crystal structure.

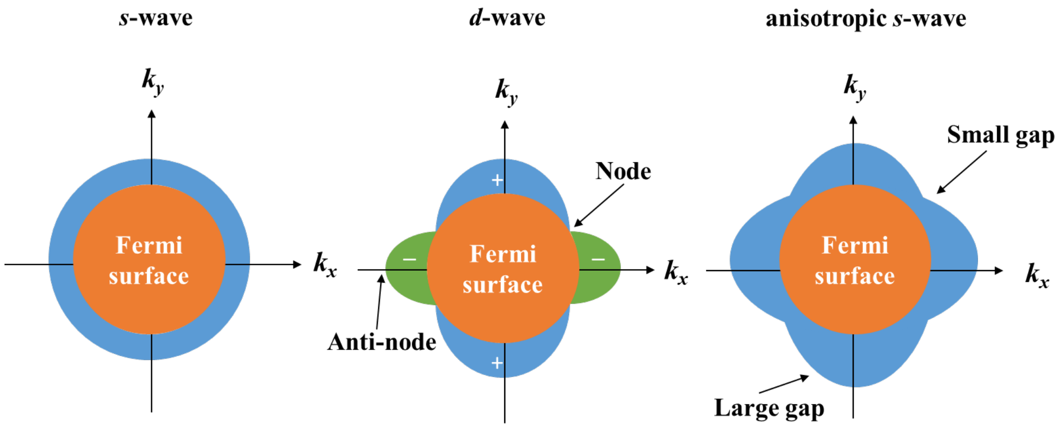

Fig. 1.18 The plot of different pairing symmetries of superconducting gap.

For BiS_2-based superconductors, discussions on superconducting gap symmetry have been made from both theoretical and experimental studies. It suggested that superconducting gap has various symmetries such as *s*-wave, *s*± wave, *d*-wave, *g*-wave from theoretical research. [45-51] On the other hand, the superconducting gap symmetry of $LaO_{0.5}F_{0.5}BiS_2$ polycrystal synthesized under high pressure by transverse-field muon spin spectroscopy measurement and the $Bi_4O_4S_3$ polycrystal by magnetic penetration depth measurement were supposed as *s*-wave with full gap. [52-53] The superconducting gap symmetry of $NdO_{1-x}F_xBiS_2$ single-crystal was proposed as *s*-wave with full gap by magnetic penetration depth and thermal transport measurements. [54-55] The superconducting gap of $LaO_{0.5}F_{0.5}BiS_{1-x}Se_x$ was found to be full gap by specific heat measurement. [56] Se-isotopic effect of $LaO_{0.6}F_{0.4}BiSSe$ also indicates that phonons do not mediate the pairing interaction and suggest unconventional superconductivity. [57] However, $LaO_{0.5}F_{0.5}BiS_2$ synthesized under ambient pressure have reported that the experimental results can be well represented by anisotropic *s*-wave and *s* + *s*-wave by transverse-field muon spin relaxation measurements. [58] From angle-resolved photoemission spectroscopy (ARPES) measurement, it showed that the superconducting gap is very anisotropic in $NdO_{0.71}F_{0.29}BiS_2$ single-crystal, and some of the gaps are observed to be almost zero like nodes. This gap structure cannot be explained by conventional superconductivity, suggesting that it is unconventional. [59] Soon after that, the superconducting gap of $LaO_{0.5}F_{0.5}BiS_2$ polycrystal was considered as *d*-wave unconventional pairing symmetry by point contact spectroscopy measurement. [44] After half a year, a concept of dirty nodal extended *s*-wave superconductivity was proposed to reconcile these two distinct experimental results of superconducting gap with a disconnected pocketlike Fermi surface structure model. [60] So far, the superconducting gap symmetry of BiS_2-based superconductors has not been fully elucidated yet.

1.5.5 The impurity effect on conventional and unconventional superconductors

One of the significant differences between conventional superconductors and unconventional superconductors is the effect of non-magnetic impurities on superconductivity, while the impurity effects of non-magnetic are greatly different depending on the superconducting gap symmetry. In the case of *s*-wave conventional superconductors, the non-magnetic impurity can scatter the Cooper pair, but the Cooper pair is symmetric with respect to the time reversal. Therefore, the density of states near the Fermi surface and the attractive force of Cooper pair formation do not change due to the non-magnetic impurities, and the T_c given by the BCS theory does not change. In the case of non-*s*-wave unconventional superconductors, T_c is greatly suppressed even by a slight lattice distortion contained in the sample. Because the SC gap of unconventional superconductors strongly depend on ***k***-space, and non-magnetic impurity scattering will change ***k*** leading to large Cooper pair breaking effects. Therefore, it is understood that the unconventional superconductor is greatly affected by the Fermi level state density when it contains a non-magnetic impurity.

It is known that when magnetic impurities are included, T_c is greatly suppressed even with a small amount. This is probably because the spins of the magnetic impurities scatter the spins of the electrons forming the Cooper pair, and the Cooper pair is broken. It can be explained as the scattering in this case is inelastic scattering and is not for time reversal.

1.6 Purpose

As above said, there are few reports of adding impurities to the Bi site on the superconducting surface in BiS_2-based superconductors. In this system, there are many discussions on the symmetry of superconductivity from various theories and experiments. But the superconducting gap symmetry of BiS_2-based superconductors is still controversial. Whether the superconductivity of this system is bulk that also is the subject of debate among scientists. So, we aimed to research the superconducting gap symmetry and superconductivity of BiS_2-based superconductors. In this work, we fabricated $LaO_{1-x}F_xBiS_2$ by flux method and investigated the symmetry and bulk properties of the superconducting gap by specific heat, electrical resistance, magnetic susceptibility, and XRD measurements. And then, we fabricated $LaO_{0.5}F_{0.5}Bi_{1-y}Sb_yS_2$ single-crystal by substituting a part of Bi on $LaO_{0.5}F_{0.5}BiS_2$ with Sb, and to investigate the impurity effect on superconductivity and the superconducting gap symmetry by same measurements.

Chapter 2

Experiment

2.1 Single-crystal and polycrystalline

The fundamental difference between single-crystal and polycrystalline is the length scale over which the atoms are related to one another by translational symmetry. Single-crystal has infinite periodicity and polycrystalline has local periodicity. An ideal single-crystal has an atomic structure that repeats periodically across its whole volume. Even at infinite length scales, each atom is related to every other equivalent atom in the structure by translational symmetry. A polycrystalline solid or polycrystal is comprised of many individual grains or crystallites. Each grain can be thought of as a single-crystal, and an interface called a grain boundary exists between the single-crystal adjacent to each other. In an isotropic polycrystalline solid, there is no relationship between neighboring grains. Therefore, on a large enough length scale, there is no periodicity across a polycrystalline sample. In a physical property study, the polycrystalline sample may be strongly affected by crystal grain boundaries due to anisotropy of the crystal structure of the sample, and a combined result of measurements in different directions may be observed sometimes. In the case of a single-crystal sample, it is expected that the observed results are ideally the essential results of the sample without any effects.

2.2 Method

Crystal growth methods can be classified into liquid phase method, gas phase method and solid phase method. Among these, from the viewpoint of growing a large single-crystal, the liquid phase method is advantageous because the easiness of rearrangement of atoms. The current methods for preparing BiS_2-based superconductors are solid phase method for polycrystalline and liquid phase method for single-crystal.

The solid phase method is a commonly used method for preparing superconductor polycrystalline. The operation is simple and easy to develop. It is a chemical reaction of solid powder at a temperature lower than the melting point, that is, a new solid solution is generated by the thermal diffusion of ions or molecules participating in the reaction. The type, purity, and property of the raw materials in the solid phase method determine the reaction temperature, reaction speed, and reaction product. The choice of raw material will be an important factor in determining the final product. At the same time, the reactants are in contact with each other during the reaction. If the size of the reactants is smaller, and the contact area between the reactant particles become larger. So, it will promote the diffusion between atoms or ions, and increase the reaction rate.

The liquid phase method is divided into melt method and solution method for preparing single-crystal. The melt method is a method of growing crystals from the same liquid phase as the composition of the target substance. In the melt method, it is necessary to heat the material to the melting point or more, but a large single-crystal can be grown in a relatively short time. After heating above the melting point, supercooling is required for single-crystal, so the cooling method is important for single-crystal. Examples of the melt method include the Bridgman method and the floating zone method. On the other hand, the solution method using a solvent is a method in which crystallization is performed by supersaturation due to slow cooling of the solution or evaporation of the solvent. In the solution method, an aqueous solution method and a hydrothermal method for growing crystals using water as a solvent are well known. However, other than water, inorganic compounds (oxides, halides, etc.) or metals that are melted at high temperatures may also be used as the solvent. The solvent is called flux, and the crystal growth method is called flux method. In this work, we used flux method on all of samples.

There are two kinds of flux methods. The components of the flux are the elements in the products; this is called as “self-flux method”. The other is the use of flux which does not include the same element in the products. The flux and raw materials for target compounds are mixed using a mortar and put in the crucible. The mixed powder is heated for the solution-growth process, and then the single-crystal is obtained. Generally, oxide materials (high-T_c cuprate compounds) are heated in open atmosphere, and non-oxide materials (Fe-based and BiS_2-based compounds) are performed in a closed atmosphere, such as sealed in a quartz tube in vacuum. Finally, the important point of flux select is the following: flux should not react with the target materials and should be easily separated from the grown single-crystal.

The advantages of the flux method are that (1) high-quality single-crystal can be grown at a temperature much lower than the melting point of the substance. (2) It has a self-shape surrounded by flat crystal faces that reflect the crystal structure as it grows. (3) Being able to grow crystals easily even if you are not familiar with the operation. And so on. On the other hand, the disadvantage of the flux method is that (1) there is a possibility that flux may be mixed as an impurity into the crystal. (2) The crystal to grow is relatively small and takes a long time to grow. And so on. The mixing of impurities can be avoided by selecting an appropriate flux. In this work, the mixture of CsCl and KCl powder was used as the flux. Because CsCl corrodes the quartz tube at a high temperature, so KCl was mixed and used.

2.3 Synthesized

The single-crystal samples of $LaO_{1-x}F_xBiS_2$ ($x = 0.5, 0.4$) and $LaO_{0.5}F_{0.5}Bi_{1-y}Sb_yS_2$ ($y = 0 \sim 0.20$) were fabricated by using flux method in vacuum quartz tubes. Powders of Bi (99.9%), Bi_2S_3 (99.99%), BiF_3 (99.9%), Bi_2O_3 (99.9%), La_2S_3 (99.9%) and Sb_2S_3 (99.9%) were used as raw materials of total 2 g, which were weighted with nominal compositions. The flux is CsCl:KCl = 5:3 molar ratio (CsCl = 11.8511 g, KCl = 3.1489 g) of total 15 g. After weighing, each of the sample and the flux was stirred for about 1 hour in air using a pestle and mortar made of alumina. Thereafter, the stirred flux was transferred to a mortar containing the sample, and further stirred for about 1 hour. The mixture of flux CsCl/KCl powders and raw materials (raw materials : flux = 1:7.5) were sealed in vacuum quartz tube. The compounds were heated at 950 ℃ for 12 h and cooled down to 600 ℃ at rate of 1.0 ℃/h by electronic Muffle furnace as shown in Fig. 2.1.

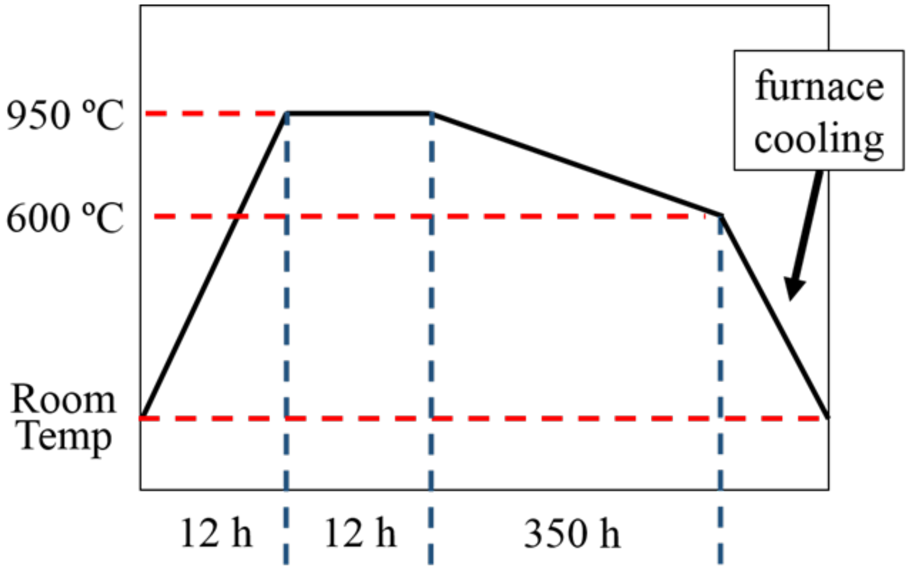

Fig. 2.1 The program of heating.

2.4 Measurements

The obtained compounds were rinsed by distilled water to take out of the flux, and then dried for 1 day at 40 °C. A plate-like sample having a size of about 1.0 mm to 2.0 mm was obtained. We performed single-crystal X-ray diffraction experiments at room temperature (~ 290 K) using a Rigaku Varimax Saturn CCD diffractometer (tube voltage: 50 kV, tube current: 24 mA). The target of this equipment is Mo-Kα ray (wavelength: 534.304 cm^{-1}). After that, the crystal structure can be measured in detail, such as bond angle, bond length, lattice parameter and so on.

In this work, the magnetic susceptibility was measured by Superconducting Quantum Interference Device (SQUID) using the Magnetic Property Measurement System (MPMS) down to 1.8 K. The electrical resistivity was measured by the four-terminal method using Quantum Design's Physical Property Measurement System

(PPMS) down to 2 K. The specific heat was measured by the relaxation method using the He^3 option of PPMS from 0.38 K to 4 K and magnetic field dependence from 0 T to 2 T.

Chapter 3

The superconductivity of $LaO_{1-x}F_xBiS_2$ ($x = 0.4, 0.5$) superconductors

The superconductivity in $LaO_{1-x}F_xBiS_2$ compounds has been studied intensively. The characteristic structure is an alternate stacking of superconducting BiS_2 layers and blocking layers (LaO/F) that for supplying electrons. The layered crystal structure is analogous to those of high-temperature (high-T_c) cuprate and Fe-based superconductors. In this chapter, we will illustrate the superconductivity of $LaO_{1-x}F_xBiS_2$ by XRD, specific heat, electrical resistivity, and magnetic susceptibility measurements.

3.1 The superconductivity of $LaO_{0.5}F_{0.5}BiS_2$

The electrical resistivity versus temperature of $LaO_{0.5}F_{0.5}BiS_2$ is shown in Fig. 3.1. The inset is the electrical resistivity of whole temperature from 2 K to 300 K. The enlarge figure is that of low temperature and the superconducting transition is observed. The electrical resistivity increases with decreasing temperature until the onset of superconducting transition, indicating semiconducting-like behavior. The value of T_c from electrical resistivity measurement is defined as the temperature where the electrical resistivity falls to 50% of its normal state, and $T_c \sim 2.7$ K.

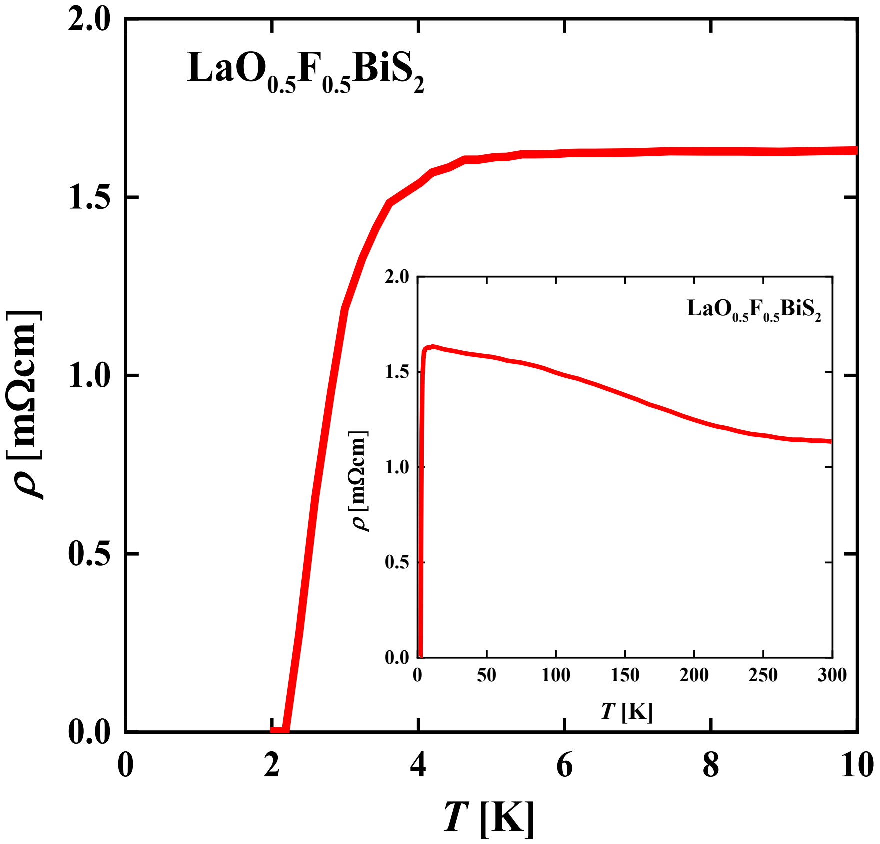

Fig. 3.1 The electrical resistivity of $LaO_{0.5}F_{0.5}BiS_2$ at low temperature. The inset is that of the range of temperature from 2 K to 300 K.

We also measured the magnetic susceptibility of $LaO_{0.5}F_{0.5}BiS_2$. Although Meissner diamagnetism was exhibited near T_c, saturation of Meissner diamagnetism could not be confirmed in the measurement temperature range. The value of T_c is determined by extrapolating to the zero level where the steepness of the Meissner diamagnetism is steepest (T_c determined by the point of intersection as shown in Fig. 3.2). The value of T_c from magnetic susceptibility measurement is about 2.7 K and it is same with that from electrical resistivity measurement.

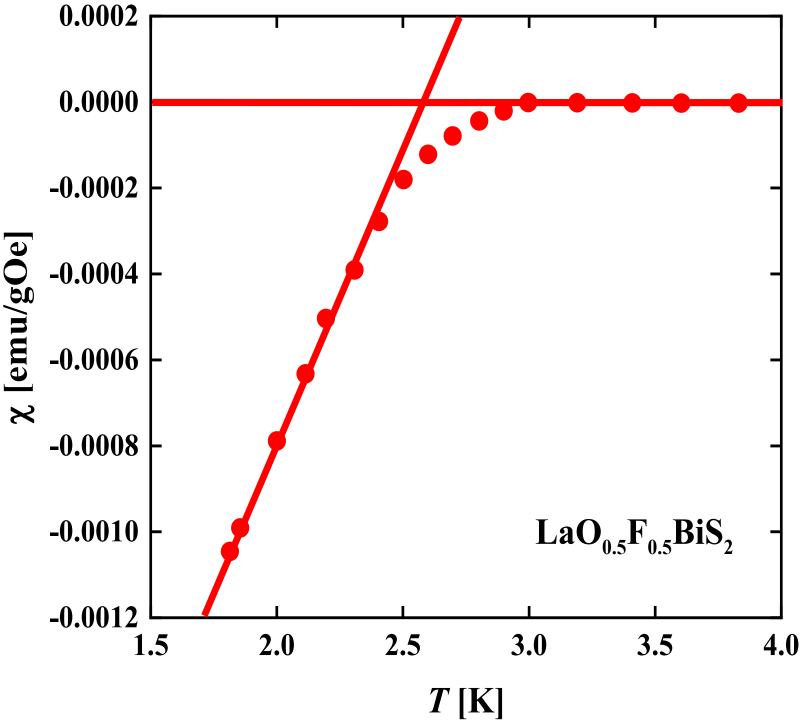

Fig. 3.2 The magnetic susceptibility of $LaO_{0.5}F_{0.5}BiS_2$ at low temperature. Solid line represents the linear fit of the data.

Figure 3.3 shows the total specific heat C divided by T, C/T, of $LaO_{1-x}F_xBiS_2$ (x = 0.5) as a function of T^2 at low temperature, and the SC transition is very clear between the normal state and the SC state indicated by the arrow. Figure 3.4 shows the C/T versus T^2 of $LaO_{1-x}F_xBiS_2$ (x = 0.5) in the normal state. The fitting result is derived by the conventional expression $C/T = \gamma_N + \beta T^2$, where γ_N is the electronic specific heat coefficient in the normal state (Sommerfeld constant) and β, the coefficient of the phonon cubic term. We obtained γ_N = 1.5 mJ/mol·K^2 and β = 1.0 mJ/mol·K^4. The coefficient β gives the Debye temperature in the simple model of phonon contribution, and it leads to Θ_D ~ 210 K ($\Theta_D = \left[\frac{12\pi^4}{5\beta}nR\right]^{\frac{1}{3}}$, where R is the gas constant and n = 5 is the number of atoms per formula unit). The γ_N value is smaller and the Θ_D value is larger than those reported for $LaO_{0.5}F_{0.5}BiSSe$. [56]

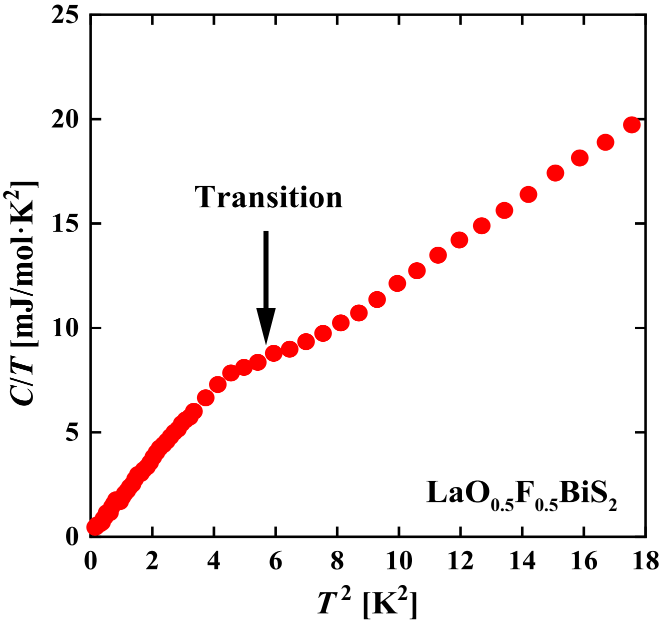

Fig. 3.3 C/T vs T^2 plot of $LaO_{0.5}F_{0.5}BiS_2$. The superconducting transition between the normal state and the SC state is indicated by the arrow.

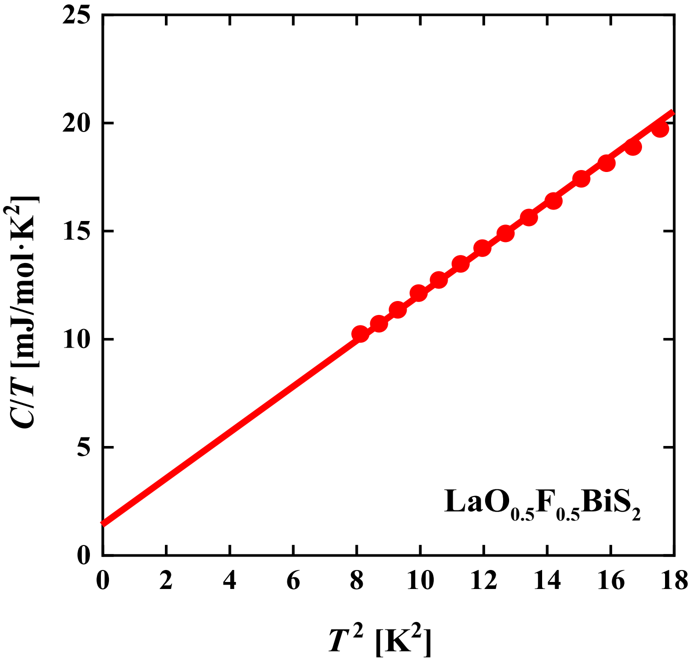

Fig. 3.4 C/T vs T^2 plot of $LaO_{0.5}F_{0.5}BiS_2$ in normal state. Solid line represents the linear fit of the data with $C/T = \gamma_N + \beta T^2$.

The electronic specific heat C_e divided by T, C_e/T, is obtained by the subtracting the phonon contribution βT^2 from C/T ($C_e/T = C/T - \beta T^2$) under the assumption that the phonon term in the normal state does not change in the SC state (Fig. 3.5). C clearly increases by ΔC at $T \sim 2.5$ K, corresponding to the SC transition. The T_c value (~2.5 K) is defined as the midpoint between the temperature at which the electronic specific heat starts to increase and its maximum temperature, and the value of T_c is a little smaller than that from electrical resistivity and magnetic susceptibility measurement. $\Delta C/\gamma_N T_c \sim 1$ is comparable to the BCS value (~1.4) when we consider the broadness of the SC transition, indicating the bulk nature of superconductivity. The BCS curve for the conventional s-wave gap in the weak-coupling limit agrees well with our specific heat results under the assumption of a small residual γ-value, γ_0, at $T << T_c$. γ_0 can be estimated to be 0.2 mJ/mol·K^2 by overall extrapolation fitting of the data with the BCS curve (Fig. 3.5). The residual γ_0-value is about 14% of the normal state γ_N-value. This fraction is almost the same as that reported for $LaO_{0.5}F_{0.5}BiSSe$. [56]

It should be noted that there is a possibility that a second gap develops in the partial density of states (DOS) giving the residual γ_0. Then assuming two bands and two gaps on each band, we fit the C_e/T versus T data based on the α-model (two-band two-gap model), which is broadly used to describe experimental data phenomenologically in many multiband superconductors such as MgB_2. [63] As shown in Fig. 3.5, the C_e/T

versus T data is well reproduced by the α-model; the size of the main gap Δ_1 and the second gap Δ_2 are $1.75k_BT_c$ and $0.36k_BT_c$. Each band is characterized by the partial Sommerfeld constant γ_1 and γ_2 in the normal state, which result in $\gamma_1 = 0.86\gamma_N$ and $\gamma_2 = 0.14\gamma_N$ by fitting. We could not find any difference in the fit for $\Delta_2 < \sim 0.36k_BT_c$, and then the Δ_2-value of $0.36k_BT_c$ will be nearly the upper bound. This result suggests the SC gap structure is two gaps with different magnitudes.

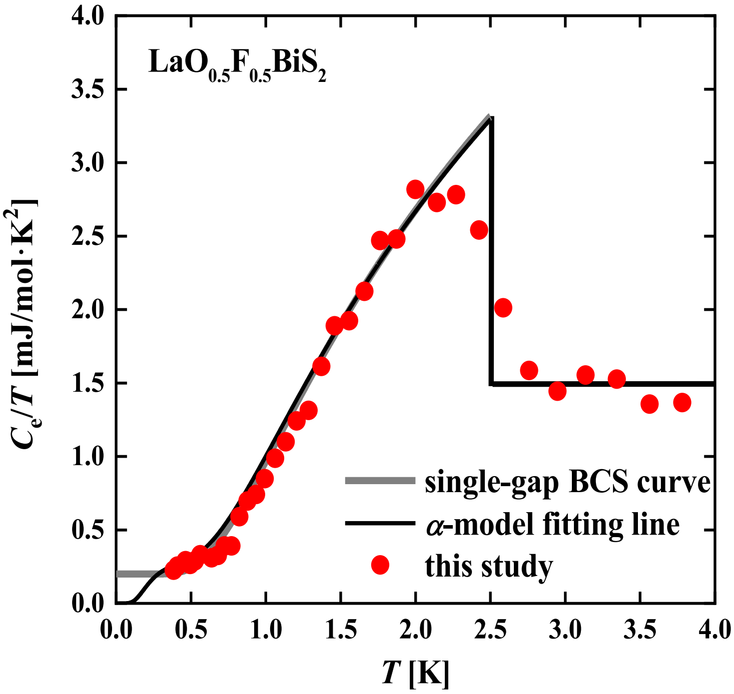

Fig. 3.5 C_e/T vs T with plot of $LaO_{0.5}F_{0.5}BiS_2$. Thick line represents the BCS curve assuming a single s-wave gap with a residual γ_0. Thin line represents the result of fit based on the α-model.

We used the typical expression $\frac{C_{es}}{T} = \frac{\gamma_N T_C a}{T} \exp\left(-\frac{\Delta(0)}{k_B T}\right)$ of BCS theory to fit the line of electronic specific heat as shown in Fig. 3.6. Based the line, we obtained two types of SC gap: one is $\Delta(0)_{small} = 0.36k_BT_c$ dominated mainly at low temperature and the other is $\Delta(0)_{\text{large}} = 1.35k_BT_c$ dominated mainly at high temperature that indicates the SC gap is anisotropic. The value of large energy gap is slightly lower than the value of 1.75 predicted by the BCS theory in the weak-coupling limit.

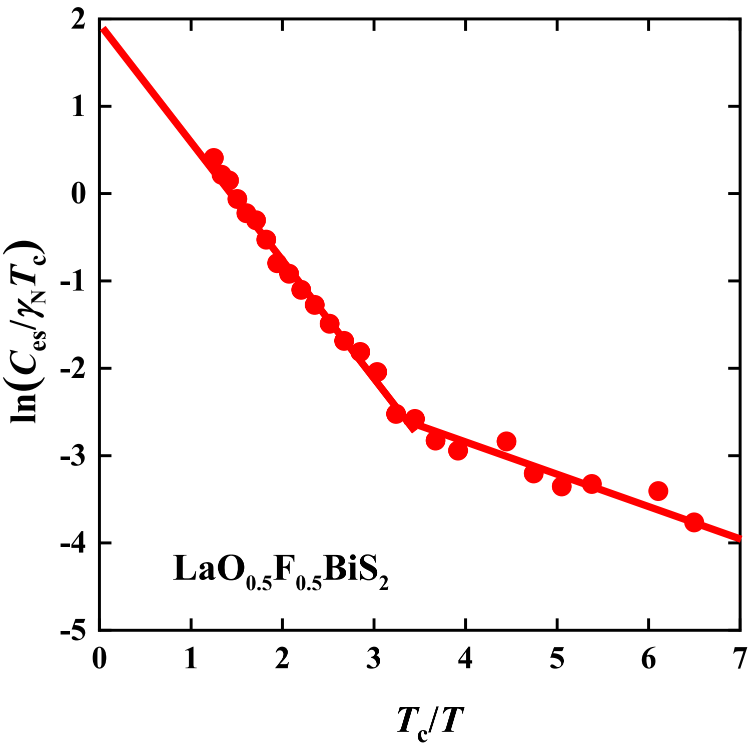

Fig. 3.6 Exponential type of electronic specific heat of $LaO_{1-x}F_xBiS_2$ (x = 0.5). Solid line represents the linear fit of the data.

But if the residual γ_0 is considered to the typical expression of the fully gapped BCS theory. The expression will change to $\frac{C_{es}}{T} - \gamma_0 = \frac{(\gamma_N - \gamma_0)T_C a}{T}\exp\left(-\frac{\Delta(0)}{k_B T}\right)$ and fit the data of the electronic specific heat at low temperatures below $T << T_c$, as shown in Fig. 3.7. Below ~$0.3T_c$, the trend of the electronic specific heat is proportional to a single exponential that shows the existence of the spectral gap. Based on the line in Fig.

3.7, we obtained the size of the spectral gap $\Delta(0) = 1.0k_BT_c$ over the low-temperature range ($T < 0.3T_c$). The ratio of Δ/k_BT_c is clearly lower than the value of 1.75 predicted by the BCS theory in the weak-coupling limit, suggesting that the gap has an anisotropy, and its smallest part is ~$1.0k_BT_c$ in magnitude. Based on α-model and BCS theory fitting results, it suggests two kinds of SC gap structure; one is an anisotropic single gap, and the other is two gaps with different magnitudes. To obtain more definitive information on the SC gap for x = 0.5, further investigation of specific heat will be necessary at lower temperatures well below ~0.3K.

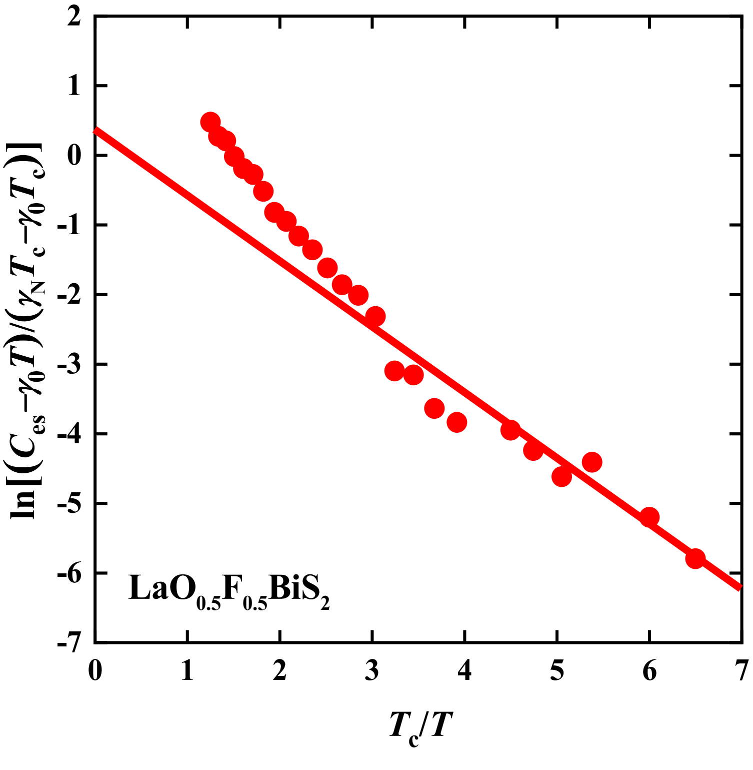

Fig. 3.7 Exponential type of electronic specific heat of $LaO_{1-x}F_xBiS_2$ (x = 0.5). Solid line represents the linear fit of the data.

Figure 3.8 shows C/T versus T^2 plots of $LaO_{1-x}F_xBiS_2$ ($x = 0.5$) under a magnetic field of 0–2 T at low temperatures. The magnitude of total specific heat is increase with the increasing magnetic field until 0.2 T, and the recovery of total specific heat is very small at magnetic field 1 T–2 T. We used the expression $\Delta\gamma = \frac{C(T,H)}{T} - \frac{C(T,0)}{T}$ to calculate the difference in the electron specific heat coefficient $\Delta\gamma$ between each magnetic field and the zero magnetic field. Figure 3.9 summarizes the chosen temperature ($T^2 = 0.15, 0.24, 0.35, 0.46\ K^2$) and magnetic field dependences of $\Delta\gamma$. $\Delta\gamma$ linearly increases for a magnetic field of 0–0.2 T despite the different temperatures, as expected with a fully gapped *s*-wave. $\Delta\gamma$ is almost nearly constant above 1 T; this is because the superconductivity is destroyed above 1 T. The electronic specific heat C_e divided by T, C_e/T, is obtained by the subtracting the phonon contribution βT^2 from C/T, as shown in Fig. 3.10. The increase in the electronic specific heat that accompanies the SC transition is suppressed by applying a magnetic field. Further, the SC gap of $LaO_{1-x}F_xBiS_2$ ($x = 0.5$) is fully gapped, as expected.

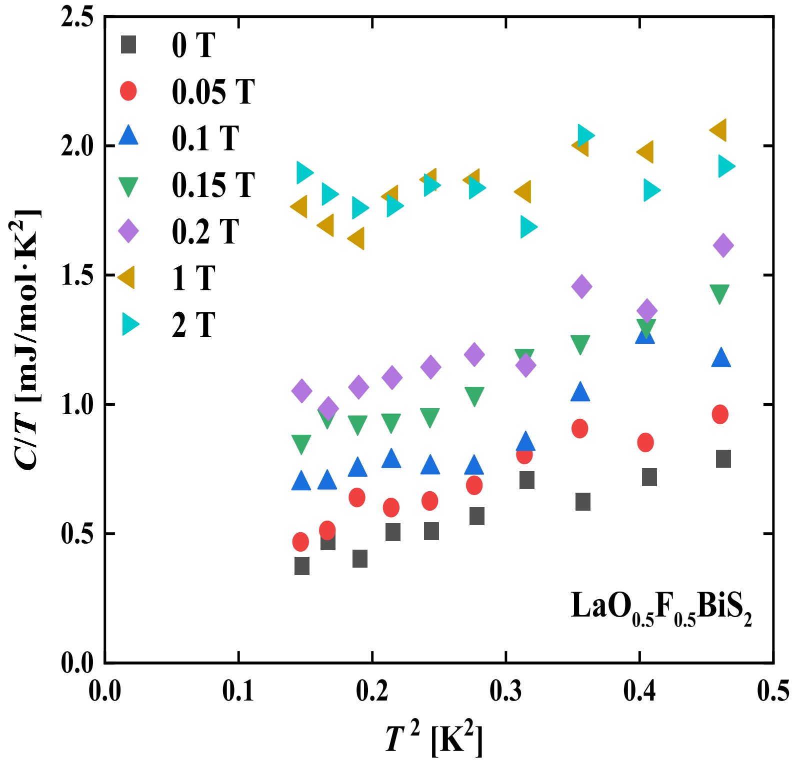

Fig. 3.8 C/T vs T^2 plot of $LaO_{0.5}F_{0.5}BiS_2$ at low temperature with magnetic field.

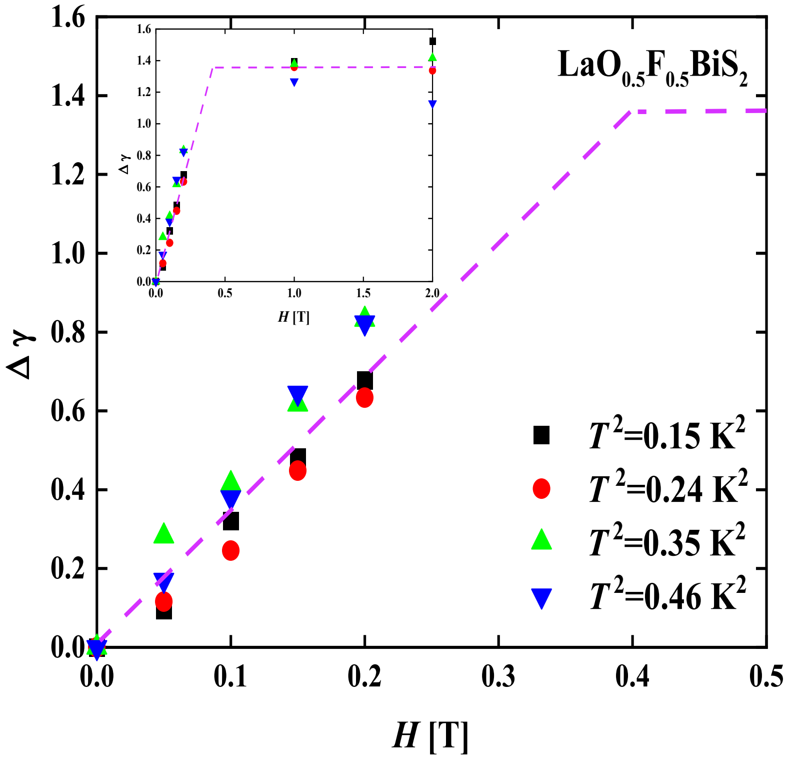

Fig. 3.9 $\Delta\gamma$ vs H of $LaO_{0.5}F_{0.5}BiS_2$. Dashed lines is guide to the eyes.

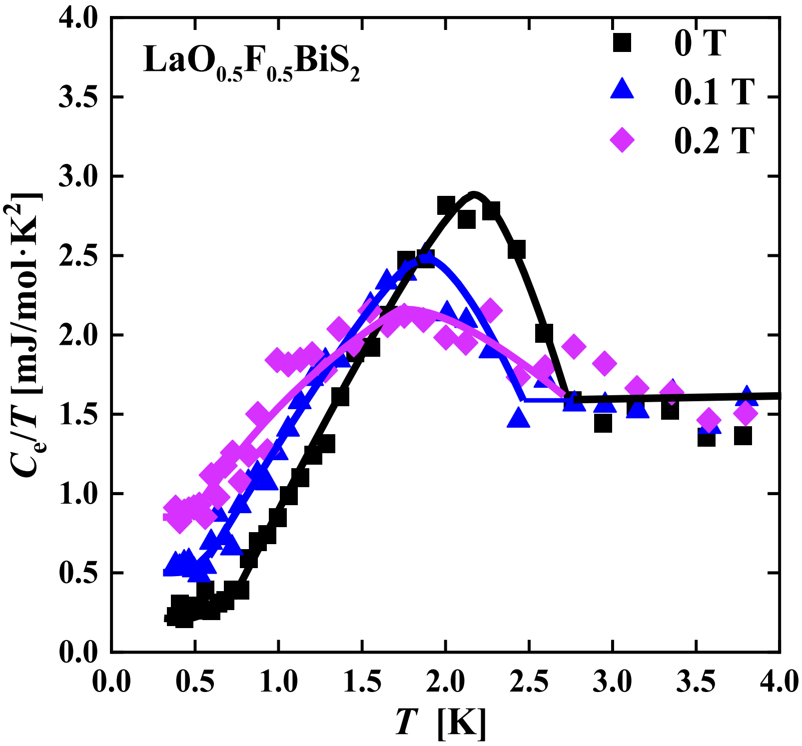

Fig. 3.10 C_e/T vs T with magnetic field of $LaO_{0.5}F_{0.5}BiS_2$. Solid lines are guides for the eyes.

3.2 The superconductivity of $LaO_{0.6}F_{0.4}BiS_2$

We measured the magnetic susceptibility of $LaO_{0.6}F_{0.4}BiS_2$. Although Meissner diamagnetism was exhibited near T_c, saturation of Meissner diamagnetism could not be confirmed in the measurement temperature range. The value of T_c is determined by extrapolating to the zero level where the steepness of the Meissner diamagnetism is steepest (T_c determined by the point of intersection as shown in Fig. 3.11). The value of T_c from magnetic susceptibility measurement is about 2.4 K.

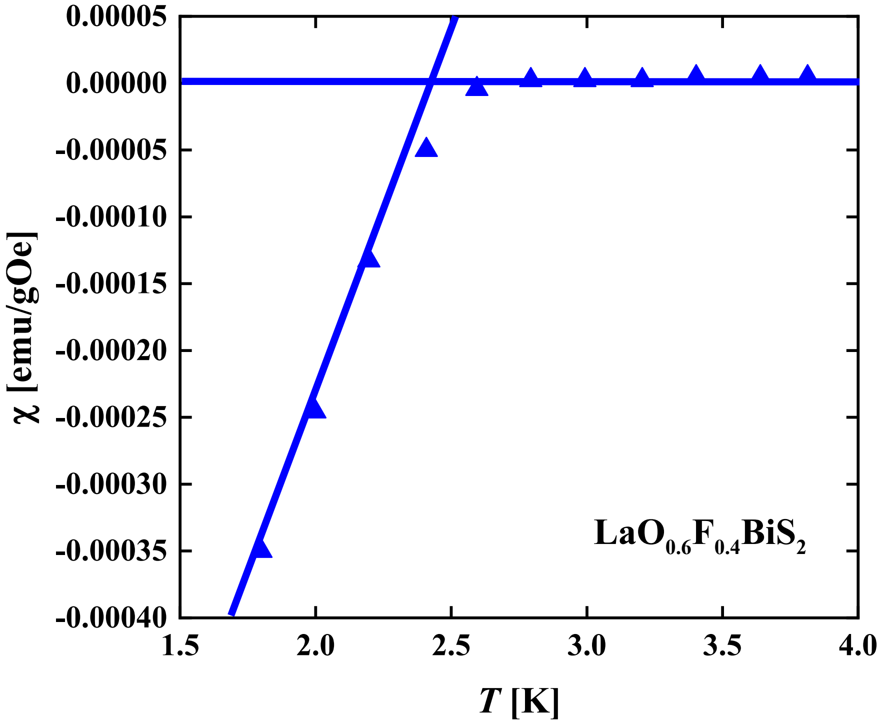

Fig. 3.11 The magnetic susceptibility of $LaO_{0.6}F_{0.4}BiS_2$ at low temperature. Solid line represents the linear fit of the data.

We conducted the same analyses for $LaO_{1-x}F_xBiS_2$ ($x = 0.4$) as those for $x = 0.5$, as shown in Fig. 3.12 and Fig. 3.13. As a result, we obtained γ_N = 1.1 mJ/mol·K^2 and β = 0.94 mJ/mol·K^4, leading to Θ_D ~ 220 K. Further, the transition between the SC state and the normal state is not as distinct as that for $LaO_{1-x}F_xBiS_2$ ($x = 0.5$) even though the γ_N and β values are almost the same.

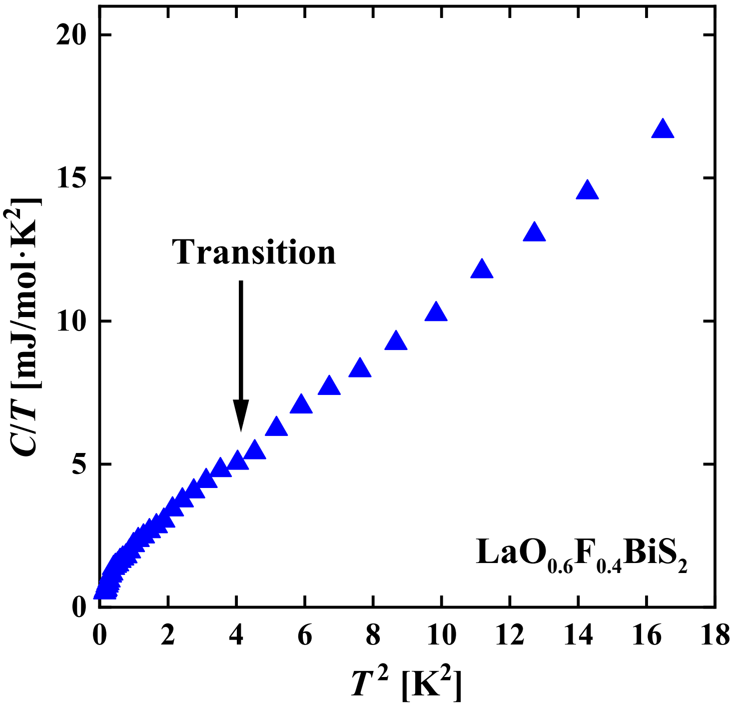

Fig. 3.12 C/T vs T^2 plot of $LaO_{0.6}F_{0.4}BiS_2$. The superconducting transition between the normal state and the SC state is indicated by the arrow.

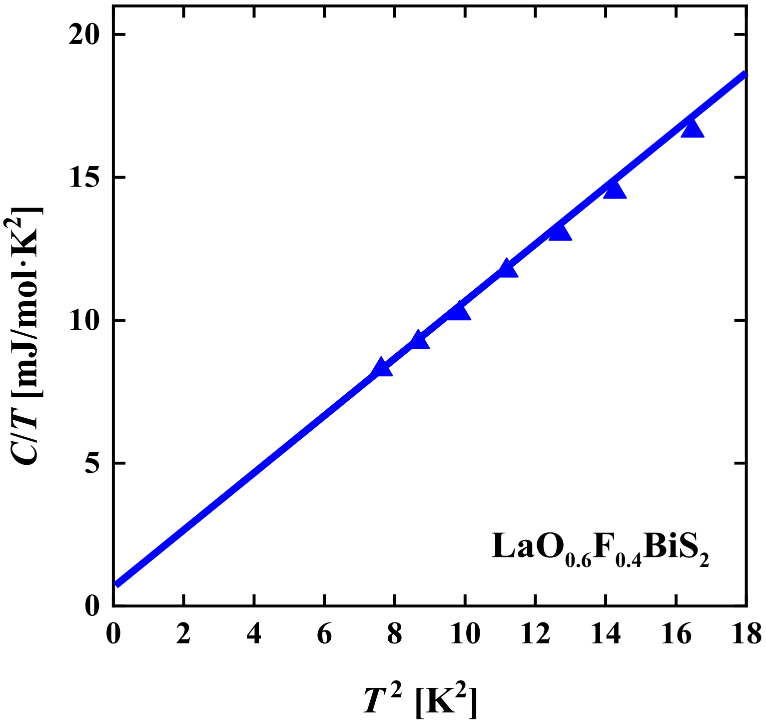

Fig. 3.13 C/T vs T^2 plot of $LaO_{0.6}F_{0.4}BiS_2$ in normal state. Solid line represents the linear fit of the data with $C/T = \gamma_N + \beta T^2$.

Figure 3.14 shows C_e/T versus T of $LaO_{1-x}F_xBiS_2$ (x = 0.4, 0.5). The magnitude of C_e/T for $LaO_{1-x}F_xBiS_2$ (x = 0.4, 0.5) in the normal state are defined as γ_N values and it is the same value with that from the fitting results of C/T in the normal state. There is an inconspicuous increase at x = 0.4 for T_c ~ 2.4 K that broadens the transition area, and the value of T_c is same with that from magnetic susceptibility measurement. Despite the broad SC transition for x = 0.4, the low-temperature specific heat for x = 0.4 seems to approach nearly zero like that for x = 0.5. This behavior suggests the bulk nature of superconductivity even for x = 0.4 although T_c is slightly suppressed and its transition is broad. A small residual γ_0 can be estimated to be 0.3 mJ/mol·K^2 by overall extrapolation fitting of the electronic specific heat data for x = 0.4.

Furthermore, in Fig. 3.14, one can see that the data for x = 0.4 largely decreases below T ~ 0.6 K (~T_c/4). Such a behavior reminds us of the SC transition in C_e/T of MgB_2, which is well understood based on two-band two-gap models. [63] Then we fit the C_e/T versus T data for x = 0.4 based on the α-model, as in x = 0.5 (Fig. 3.14). The characteristic T-dependence of C_e/T for x = 0.4 below ~T_c is well reproduced by the α-model. The parameters obtained from the fit are as follows; $\Delta_1 = 1.75k_BT_c$, $\Delta_2 = 0.60k_BT_c$, $\gamma_1 = 0.40\gamma_N$, and $\gamma_2 = 0.60\gamma_N$. The contributions to C_e from two bands are closer in x = 0.4, which are largely different in the data for x = 0.5. This result suggests the two-gap effect is more dominant for x = 0.4.

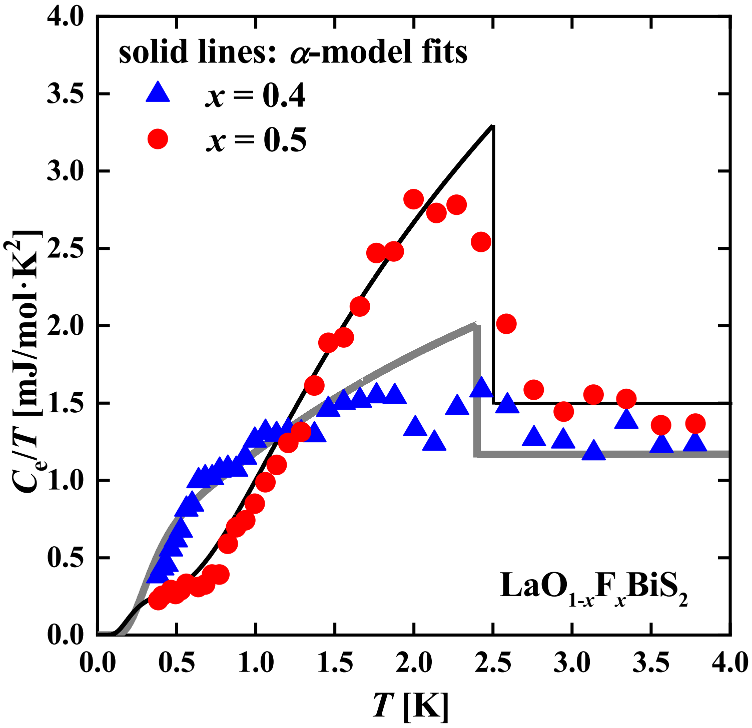

Fig. 3.14 C_e/T vs T of $LaO_{1-x}F_xBiS_2$ (x = 0.4, 0.5). Solid lines represent the results of the α-model fits.

We also used the typical expression $\frac{C_{\mathrm{es}}}{T} = \frac{\gamma_{\mathrm{N}} T_{\mathrm{C}} a}{T} \exp\left(-\frac{\Delta(0)}{k_{\mathrm{B}} T}\right)$ of BCS theory to fit the line of electronic specific heat of $LaO_{1-x}F_xBiS_2$ (x = 0.4) as shown in Fig. 3.15. Based the line in Fig. 3.15, we obtained the size of SC gap $\Delta(0) = 0.63k_BT_c$ dominated at whole temperature, suggesting that the gap has an isotropy. The ratio of Δ/k_BT_c is too much lower than the value of 1.75 predicted by the BCS theory in the weak-coupling limit.

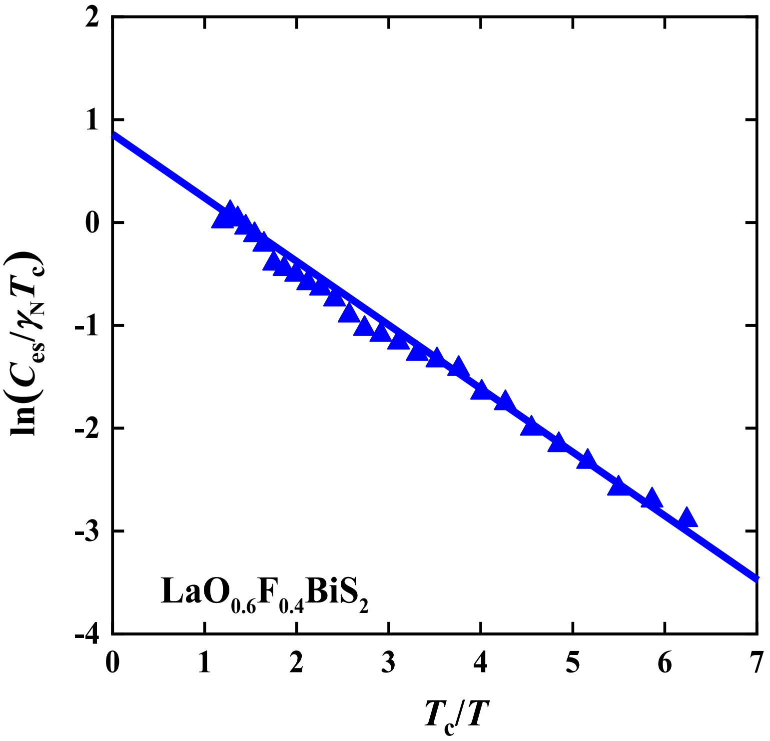

Fig. 3.15 Exponential type of electronic specific heat of $LaO_{1-x}F_xBiS_2$ ($x = 0.4$). Solid line represents the linear fit of the data.

But if the residual γ_0 is considered $\frac{C_{es}}{T} - \gamma_0 = \frac{(\gamma_N - \gamma_0)T_C a}{T} \exp\left(-\frac{\Delta(0)}{k_B T}\right)$ and fit the data of the electronic specific heat at low temperatures below $T << T_c$, as shown in Fig. 3.16. We obtained the size of the SC gap $\Delta(0) = 1.08 k_B T_c$ over the low-temperature range ($T < 0.3T_c$). The ratio of $\Delta/k_B T_c$ is lower than the value of 1.75 predicted by the BCS theory in the weak-coupling limit, but it is almost same value as the SC gap of $LaO_{1-x}F_xBiS_2$ ($x = 0.5$) in magnitude over the low-temperature range ($T < 0.3T_c$). Based on α-model and BCS theory fitting results, it suggests two kinds of SC gap structure; one is an isotropic single gap, and the other is two gaps with closer contribution to C_e. The two-gap effect is more dominant for $x = 0.4$, which are largely different with $x =$

0.5.

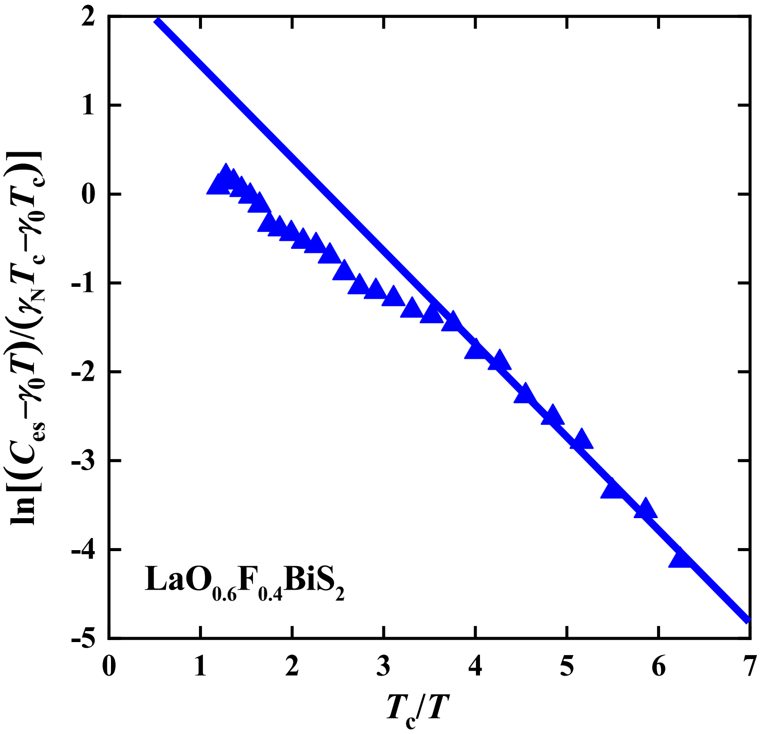

Fig. 3.16 Exponential type of electronic specific heat of $LaO_{1-x}F_xBiS_2$ (x = 0.4). Solid line represents the linear fit of the data.

3.3 The XRD results of $LaO_{1-x}F_xBiS_2$ (x = 0.4, 0.5)

We performed the single-crystal X-ray diffraction experiments of $LaO_{1-x}F_xBiS_2$ (x = 0.4, 0.5) using a Rigaku Varimax Saturn CCD diffractometer at room temperature (~290 K). The crystal structure shows tetragonal symmetry with the $P4/nmm$ space group in these two compounds. The data of crystal structure are shown in Table 3.1, and all the data of $LaO_{1-x}F_xBiS_2$ (x = 0.4, 0.5) are almost same. The in-plane chemical pressure coefficient, given by (R_{Bi}+R_{S1})/(Bi-S1(in-plane) distance), was proposed by Mizuguchi group, [42] where R_{Bi} = 104.19 pm and R_{S1} = 184 pm are the ionic radius of

Bi and S in the Bi-S1 plane. The Bi-S1(in-plane) distance is almost constant (~2.87 Å), independent of x. Then the in-plane chemical pressure coefficient was calculated to be 1.005. These results indicate that the in-plane chemical pressure effect is very weak in these two compounds.

Table 3.1 List of crystal structure of $LaO_{1-x}F_xBiS_2$ ($x = 0.4, 0.5$).

x	0.4	0.5
a [Å]	4.0674	4.0655
c [Å]	13.448	13.433
c/a [-]	3.3063	3.3041
V [Å^3]	222.49	222.03
Bi-S1 [Å]	2.8761	2.8748
Bi-S2 [Å]	2.530	2.530
La-S1 [Å]	3.735	3.748
La-S2 [Å]	3.867	3.862
S1-Bi-S1 [°]	179.61	180.38

3.4 Discussions and conclusions of $LaO_{1-x}F_xBiS_2$ ($x = 0.4, 0.5$)

From the above results of $LaO_{1-x}F_xBiS_2$ ($x = 0.4, 0.5$), we consider that the fluorine concentration of $LaO_{1-x}F_xBiS_2$ is what makes the two samples different. Fluorine doping can influence whether the transition area becomes broad, and 40% fluorine doping may be the boundary in these compounds at which the nature of the superconductivity starts worsening. This boundary may be related to the boundary between the bulk and the nonbulk of SC, as reported previously, [61, 37] although the fluorine concentration at the boundary is slightly different. The fluorine concentration of our single-crystal samples was nominal, and unfortunately, it is very difficult to determine the exact net fluorine concentration because of light element. We speculate that if the SC nature collapses at a certain doping level x, its doping level will be below net $x = 0.4$.

The results of temperature and magnetic field dependence in the electronic specific heat below T_c indicate that $LaO_{1-x}F_xBiS_2$ ($x = 0.5$) is a fully gapped *s*-wave superconductor in the weak coupling limit, are consistent with those reported in magnetic penetration depth [53] and thermal conductivity [55] experiments. The results also indicate that $LaO_{1-x}F_xBiS_2$ ($x = 0.4$) shows bulk superconductivity in a manner similar to $LaO_{1-x}F_xBiS_2$ ($x = 0.5$), although T_c is slightly suppressed and has a broad transition.

The α-model results of $LaO_{1-x}F_xBiS_2$ ($x = 0.5$) suggest the SC gap structure is two gaps with different magnitudes. However, from the BCS theory fitting results, it has two types of SC gap: one is $\Delta(0)_{small} = 0.36k_BT_c$ and the other is $\Delta(0)_{large} = 1.35k_BT_c$ that indicates the SC gap is anisotropic. These BCS theory fitting results agree with that of $NdO_{0.71}F_{0.29}BiS_2$ from ARPES, [59] and from that ARPES results, a very small SC gap of about $0.1k_BT_c$ was observed, so a value of $0.36k_BT_c$ may be essential. But if the small residual γ_0 is considered, the size of SC gap has become $1.0k_BT_c$ over the low-temperature range ($T < 0.3T_c$), suggesting that the gap has an anisotropy, and its smallest part is ~ $1.0k_BT_c$ in magnitude. Based on α-model and BCS theory fitting results, it suggests two kinds of SC gap structure; one is an anisotropic single gap, and the other is two gaps with different magnitudes.

The α-model results of $LaO_{1-x}F_xBiS_2$ (x = 0.4) suggest that the contributions to C_e from two bands are closer in x = 0.4. However, from the BCS theory fitting results, we obtained the size of SC gap $\Delta(0) = 0.63k_BT_c$ dominated at whole temperature, suggesting that the gap has an isotropy. The ratio of Δ/k_BT_c is too much lower than the value of 1.75 predicted by the BCS theory in the weak-coupling limit. But if the small residual γ_0 is considered, the size of SC gap has become $1.08k_BT_c$ over the low-temperature range ($T < 0.3T_c$). The ratio of Δ/k_BT_c is lower than the value of 1.75 predicted by the BCS theory in the weak-coupling limit, but it is almost same value as the SC gap of $LaO_{1-x}F_xBiS_2$ (x = 0.5) in magnitude over the low-temperature range ($T < 0.3T_c$). Based on α-model and BCS theory fitting results, it suggests two kinds of SC gap structure; one is an isotropic single gap, and the other is two gaps with closer contribution to C_e. The two-gap effect is more dominant for x = 0.4, which are largely different with x = 0.5.

Chapter 4

The superconductivity of $LaO_{0.5}F_{0.5}Bi_{1-y}Sb_yS_2$ (y = 0–0.2) superconductors

There are few reports of adding impurities to the Bi site on the superconducting surface in BiS_2-based superconductors. The superconductivity of $LaO_{0.5}F_{0.5}BiS_2$ is very robust for investigating the impurity effect. So, in this chapter, we will study the impurity effects on superconductivity of $LaO_{0.5}F_{0.5}Bi_{1-y}Sb_yS_2$ (y = 0–0.2) by XRD, specific heat, electrical resistivity, and magnetic susceptibility measurements.

4.1 The XRD results of $LaO_{0.5}F_{0.5}Bi_{1-y}Sb_yS_2$ (y = 0–0.2)

We examined the single-crystal X-ray diffraction patterns of $LaO_{0.5}F_{0.5}Bi_{1-y}Sb_yS_2$ (y = 0–0.20) at room temperature (~290 K) as shown in Table 4.1 in detail. The crystal structure shows tetragonal symmetry with the $P4/nmm$ space group as well as Sb-free crystals. Figure 4.1 shows the Sb-concentration dependences of the lattice parameters a and c. The c-axis is nearly independent of y, whereas the a-axis slightly decreases with increasing y because of the smaller ion radius of Sb^{3+}. The Mizuguchi group [42] proposed the in-plane chemical pressure coefficient, given by $(R_{Bi} + R_{S1})$/(Bi-S1(in-plane) distance), as a measure of chemical pressure within the BiS_2 plane, where R_{Bi} = 104.19 pm and R_{S1} = 184 pm are the ionic radii of Bi and S in the Bi-S1 plane, respectively. The Bi-S1(in-plane) distance is almost constant (~2.87 Å), independent of y, and the in-plane chemical pressure coefficient was calculated to be 1.005. These results indicate that the in-plane chemical pressure is positive but very weak in these compounds and that impurity scattering plays an essential role in tuning the electronic state in these compounds.

Table 4.1 List of crystal structure of $LaO_{0.5}F_{0.5}Bi_{1-y}Sb_yS_2$ (y = 0–0.2).

y	a [Å]	c [Å]	V [Å^3]	Bi-S1 [Å]	Bi-S2 [Å]	La-S1 [Å]	La-S2 [Å]	S1-Bi-S1 [°]
0	4.0655	13.433	222.03	2.8748	2.530	3.748	3.862	179.40
0.02	4.0685	13.367	221.26	2.8771	2.537	3.685	3.867	181.37
0.04	4.0724	13.399	222.10	2.8797	2.532	3.686	3.871	181.05
0.06	4.0690	13.361	221.20	2.8774	2.529	3.681	3.874	181.28
0.08	4.0701	13.395	221.89	2.8781	2.532	3.685	3.86	180.80
0.10	4.0647	13.369	220.88	2.8744	2.525	3.671	3.857	181.28
0.12	4.0681	13.363	221.15	2.8768	2.520	3.661	3.855	181.54
0.14	4.0689	13.374	221.41	2.8774	2.517	3.659	3.856	181.60
0.16	4.0702	13.355	221.25	2.8785	2.521	3.646	3.854	182.00
0.18	4.0697	13.361	221.29	2.878	2.514	3.655	3.855	181.60
0.20	4.0716	13.354	221.39	2.8793	2.511	3.658	3.846	181.40

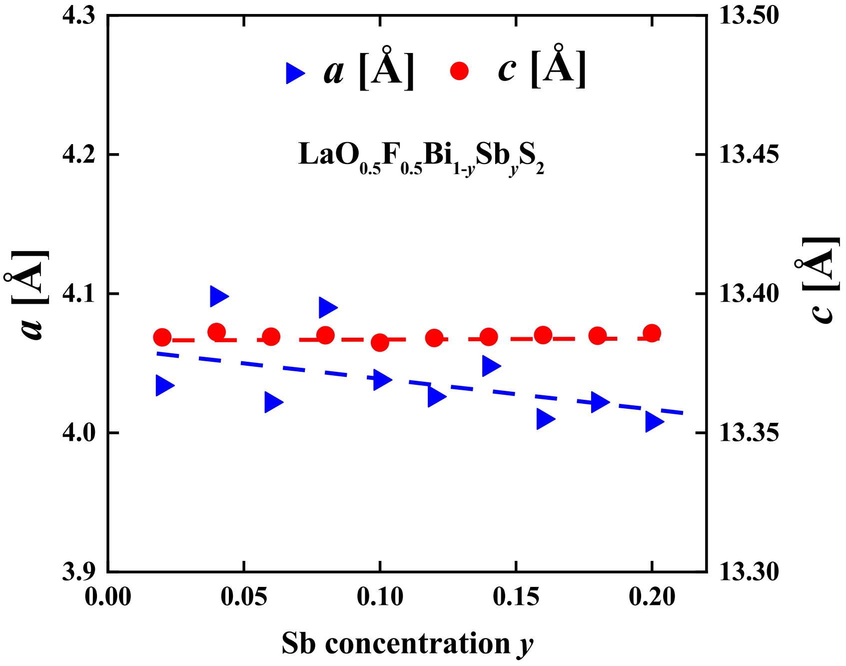

Fig. 4.1 Lattice parameters a and c of $LaO_{0.5}F_{0.5}Bi_{1-y}Sb_yS_2$. Dashed lines are guides for the eyes.

4.2 The magnetic susceptibility results of $LaO_{0.5}F_{0.5}Bi_{1-y}Sb_yS_2$ (y = 0–0.2)

We measured the magnetic susceptibility of $LaO_{0.5}F_{0.5}Bi_{1-y}Sb_yS_2$ (y = 0–0.2) normalized by its minimum magnetic susceptibility at lowest temperature respectively, and Meissner diamagnetism was exhibited near T_c. The value of T_c is determined by extrapolating to the zero level where the steepness of the Meissner diamagnetism is steepest (T_c determined by the point of intersection as shown in Fig. 4.2). The values of T_c are 2.7 K, 2.4 K, and 2.1 K for y = 0, 0.06, and 0.12, respectively. The transition temperature is suppressed by Sb substitution.

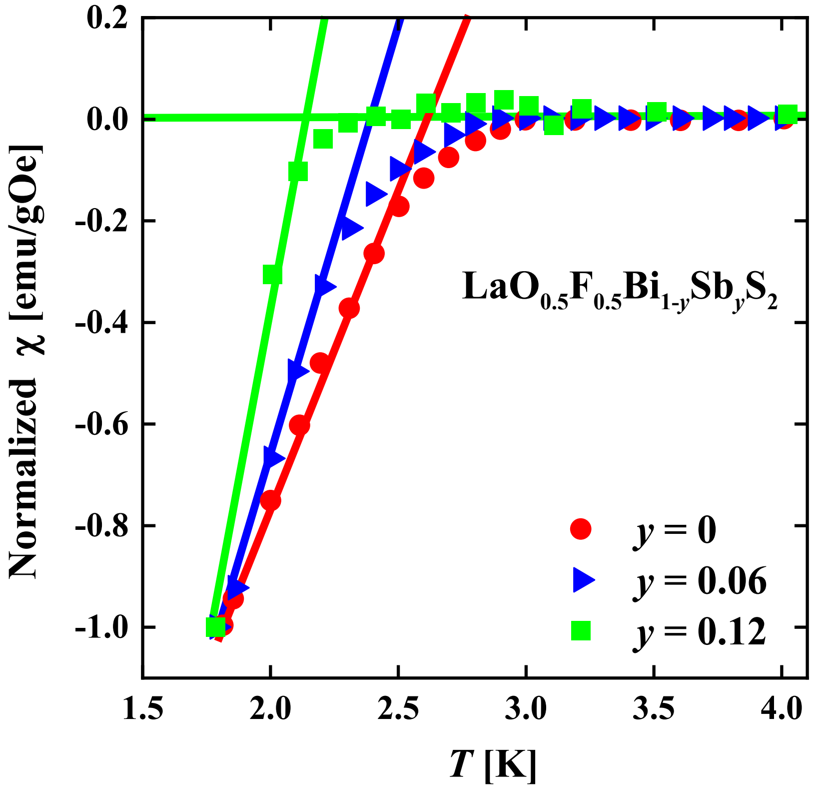

Fig. 4.2 The normalized magnetic susceptibility of $LaO_{0.5}F_{0.5}Bi_{1-y}Sb_yS_2$ at low temperature.

4.3 The electrical resistivity results of $LaO_{0.5}F_{0.5}Bi_{1-y}Sb_yS_2$ (y = 0–0.2)

The electrical resistivity ρ versus T of $LaO_{0.5}F_{0.5}Bi_{1-y}Sb_yS_2$ (y = 0–0.20) are shown in Fig. 4.3, The superconducting transition is observed in y = 0, 0.02 and 0.10. The electrical resistivity ρ increases with decreasing temperature in all samples until the onset of superconducting transition, indicating semiconducting-like behavior. Such a semiconducting-like behavior becomes much stronger with the Sb substitution. The amplitude of increase become much bigger in y = 0.18 and 0.20 while the superconductivity is not observed in these compounds. The value of T_c is defined as the temperature at which the electrical resistivity decreases to 50% of its normal state value just above the SC transition. The values of T_c are 2.7 K and 2.6 K for y = 0 and 0.02 respectively as shown in Fig. 4.4 at low temperature. The resistivity for Sb-doped samples shows an increase at low temperatures, suggesting a carrier localization due to impurities. Such a carrier localization can enhance the electron correlation, usually suppressing of T_c. [62] The slight decrease in T_c in Sb-doped samples can be ascribed to the enhancement of electron correlations due to the weak localization of carriers.

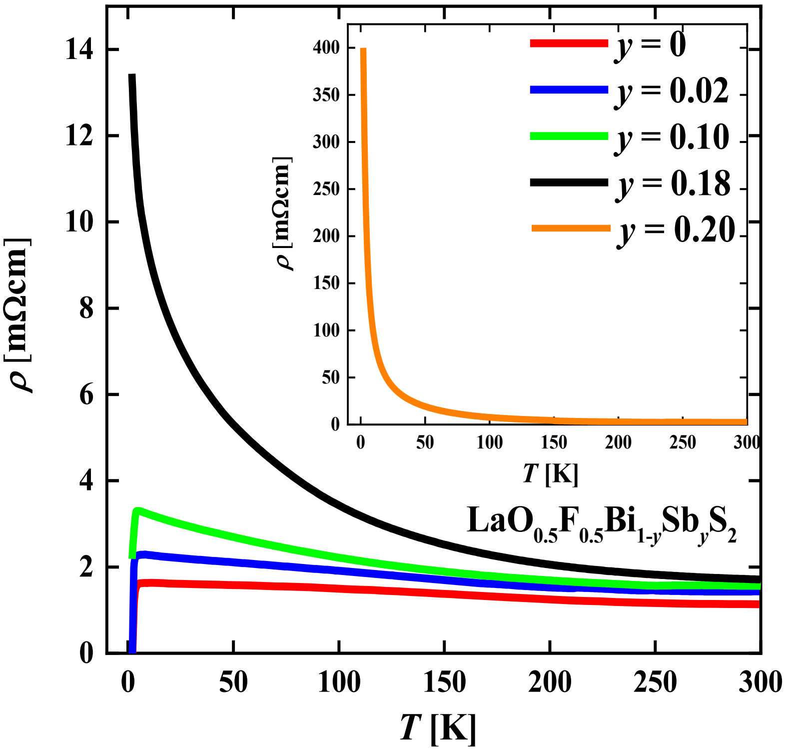

Fig. 4.3 ρ vs T of $LaO_{0.5}F_{0.5}Bi_{1-y}Sb_yS_2$ from 2 K to 300 K.

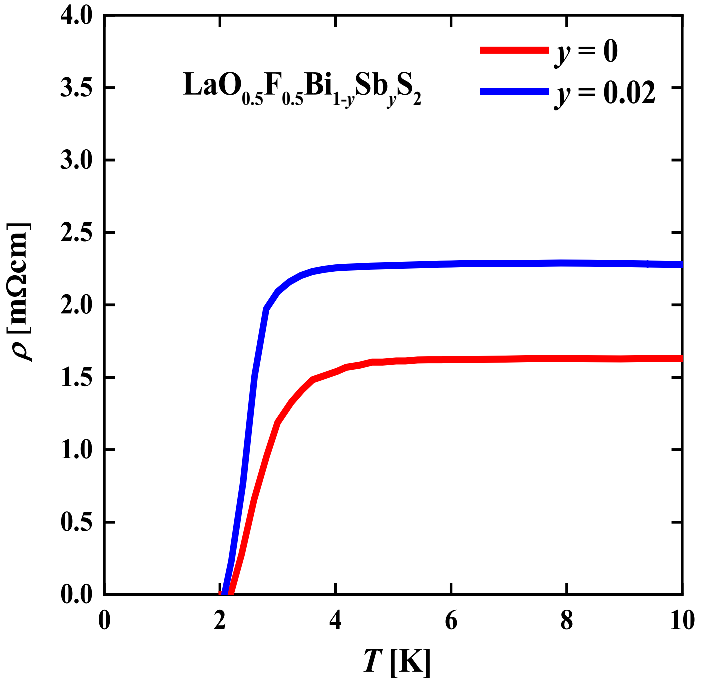

Fig. 4.4 ρ vs T of $LaO_{0.5}F_{0.5}Bi_{1-y}Sb_yS_2$($y$ = 0, 0.02) at low temperature.

4.4 The specific heat results of $LaO_{0.5}F_{0.5}Bi_{1-y}Sb_yS_2$ (y = 0–0.2)

Figure 4.5 shows the C_e/T versus T plots of $LaO_{0.5}F_{0.5}Bi_{1-y}Sb_yS_2$ (y = 0–0.20). The C_e/T values for y = 0, 0.06, and 0.12 show clear SC transition anomalies. The sample for y = 0.20 does not show any signs of bulk superconductivity. Here, T_c is defined as the midpoint between the temperature at which the electronic specific heat starts to increase and its maximum temperature, and its value is 2.5, 2.2, and 1.7 K for y = 0, 0.06, and 0.12, respectively. These T_c values are consistent with those from electrical resistivity and magnetic susceptibility measurements, as shown in Fig. 4.6. The transition temperature is suppressed by impurity scattering in both the specific heat and the electrical resistivity and magnetic susceptibility measurements. The rate of decrease in T_c owing to non-magnetic impurities is at least ~0.02/Sb% at low Sb concentrations. The slight decrease in T_c in Sb-doped samples can be ascribed to the enhancement of electron correlations due to the weak localization of carriers. The inset of Fig. 4.6 shows T_c versus abovementioned in-plane chemical pressure compared with Mizuguchi group. [42] Based the results of Mizuguchi group, the transition temperature increases with increasing in-plane chemical pressure. So, it is impossible for T_c to rise by Sb substitution, because the in-plane chemical pressure is very weak in this work.

As mentioned in the chapter 3, the secondary gap Δ_2 for $x = 0.5$ obtained assuming the alpha model is very small (< ~$0.36k_BT_c$), meaning that the T-dependence of C_e/T at $T > 0.3$ K is mainly dominated by the main gap in the case of the two-gap superconductivity. Then, in Fig. 4.5, we simply fit the data for Sb-doped samples to the single-gap BCS curve in the weak-coupling limit with a residual γ_0. The C_e/T for y = 0.06 is very similar to that for pure sample (y = 0) except for the difference of T_c. This result means that Sb-doping of y = 0.06 has no effect on the gap structure.

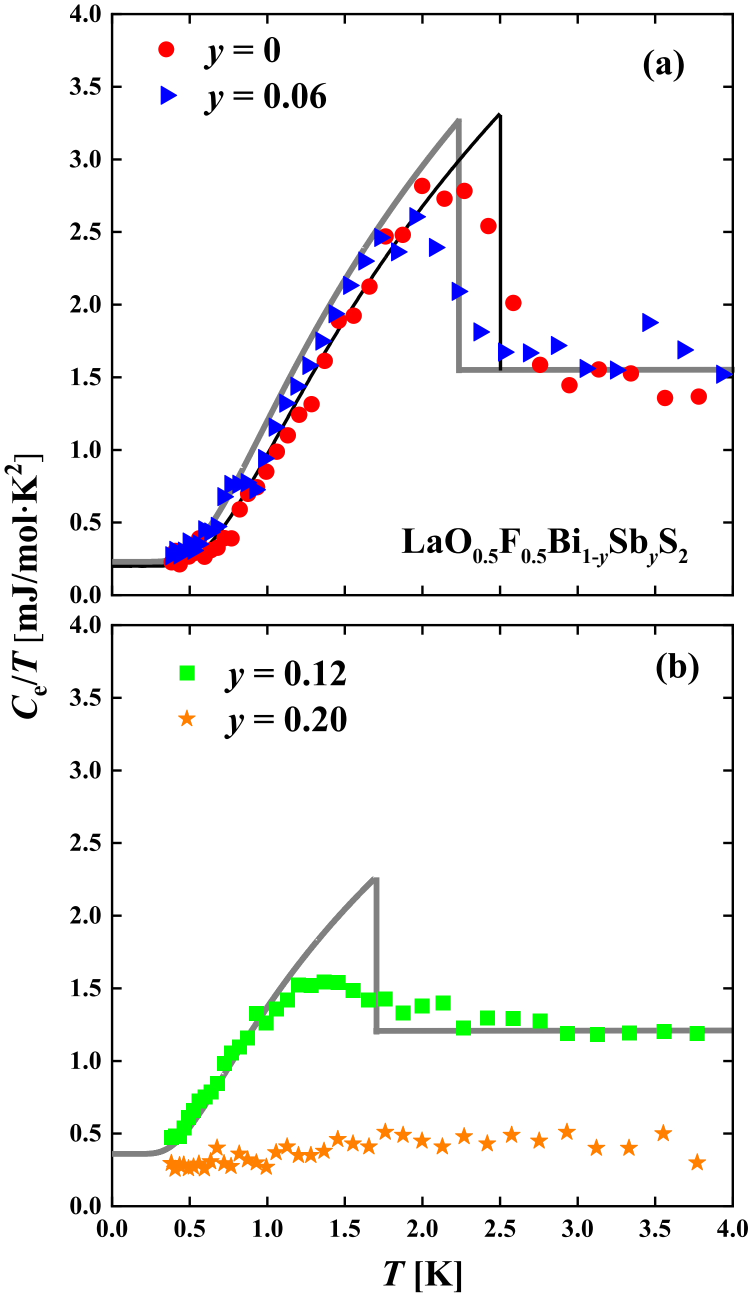

Fig. 4.5 C_e/T vs T of $LaO_{0.5}F_{0.5}Bi_{1-y}Sb_yS_2$. Solid lines represent the BCS curve assuming a single *s*-wave gap with a residual γ_0.

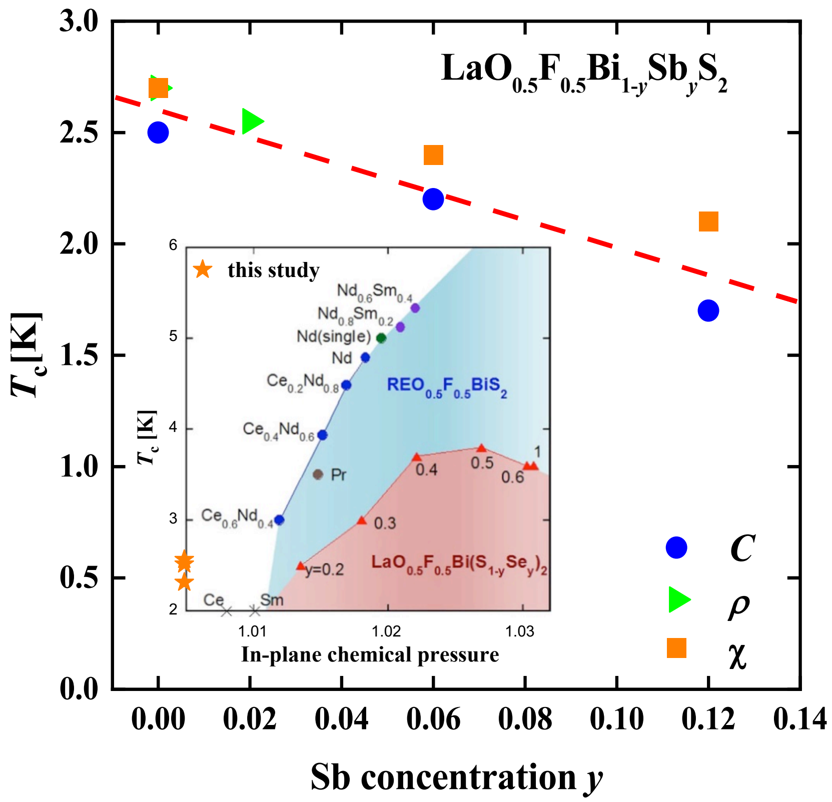

Fig. 4.6 T_c vs Sb concentration of $LaO_{0.5}F_{0.5}Bi_{1-y}Sb_yS_2$. Dashed lines are guides for the eyes. Inset: T_c vs in-plane chemical pressure with plot of this study and Mizuguchi group's study.

Figure 4.7 shows the Sb-doping dependences of γ_N and γ_0, where γ_N is defined as the magnitude of C_e/T in the normal state, and the residual linear term γ_0 is obtained by extrapolating C_e/T at low temperatures to 0 K. The γ_0-value is hardly affected below y = 0.06, even though the substitution of Sb suppresses the superconductivity, indicating that the density of states at the Fermi level in the SC state is not recovered by Sb-doping. The robustness of the SC gap against the pair-breaking due to non-magnetic impurities means that the SC gap is consistent with a full gap with an s-wave symmetry. The γ_N-value remains nearly constant until $y \sim 0.1$. However, the γ_N-value is strongly suppressed by Sb-doping above $y \sim 0.12$, where the resistivity increases considerably at low temperatures.

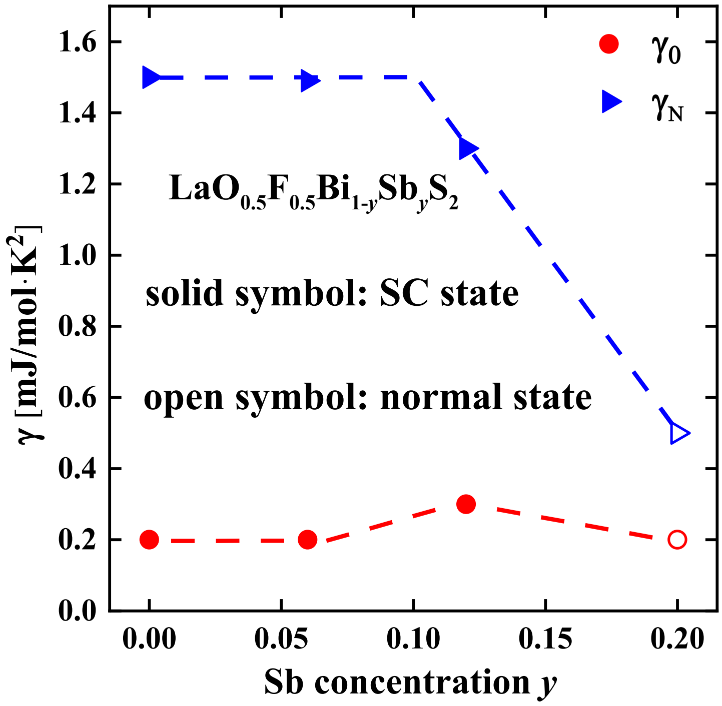

Fig. 4.7 γ vs Sb concentration for $LaO_{0.5}F_{0.5}Bi_{1-y}Sb_yS_2$.

4.5 The comparison of $LaO_{0.5}F_{0.5}Bi_{1-y}Sb_yS_2$ (y = 0, 0.06)

Figure 4.8 shows the total specific heat C divided by T, C/T, of $LaO_{0.5}F_{0.5}Bi_{1-y}Sb_yS_2$ (y = 0, 0.06) as a function of T^2 at low temperature, and the SC transition is very clear between the normal state and the SC state in both two samples indicated by the arrow although the transition has a little shift. Figure 4.9 shows the C/T versus T^2 of $LaO_{0.5}F_{0.5}Bi_{1-y}Sb_yS_2$ (y = 0, 0.06) in the normal state. The fitting result is derived by the conventional expression $C/T = \gamma_N + \beta T^2$, we obtained γ_N = 1.5 mJ/mol·K^2 and β = 0.9 mJ/mol·K^4, leading to $\Theta_D \sim 220$ K for y = 0.06. The γ_N value is same and the Θ_D value is a little larger than those values of y = 0.

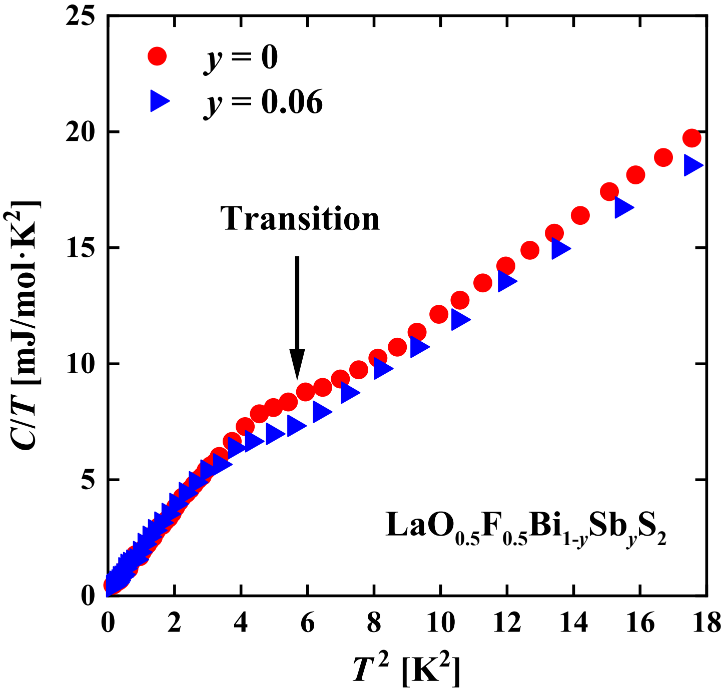

Fig. 4.8 C/T vs T^2 plot of $LaO_{0.5}F_{0.5}Bi_{1-y}Sb_yS_2$. The superconducting transition between the normal state and the SC state is indicated by the arrow.

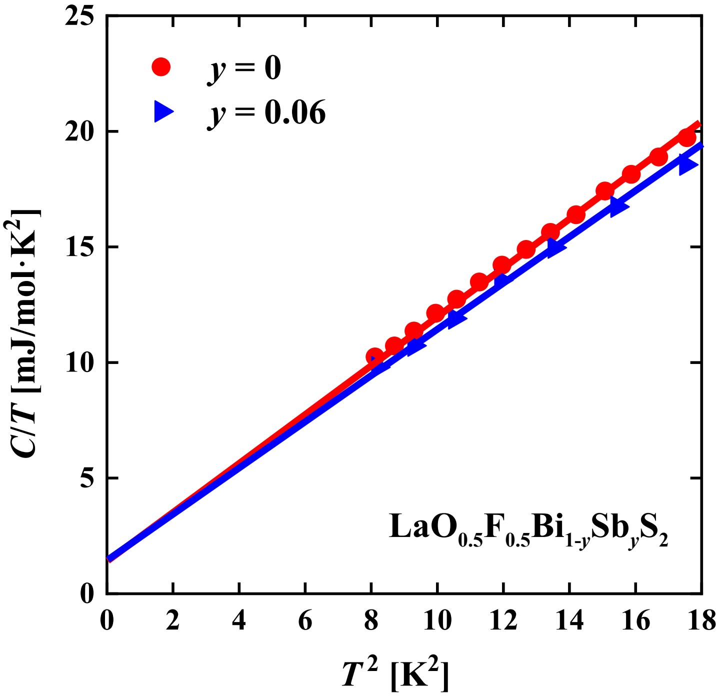

Fig. 4.9 C/T vs T^2 plot of $LaO_{0.5}F_{0.5}Bi_{1-y}Sb_yS_2$ in normal state. Solid line represents the linear fit of the data with $C/T = \gamma_N + \beta T^2$.

We analyzed C_e/T versus T/T_c for y = 0, 0.06 as shown in Fig. 4.10, where the temperature is normalized by T_c. The T-dependence of C_e/T between y = 0 and 0.06 is coincident below T_c. C_e is well known to have two components in the SC state: the thermal excitation of quasi-particles beyond the gap as the temperature changes and the effect of the T-dependence of the gap size. The present C_e/T results for y = 0 and 0.06 mean that both components in C_e are almost identical for the y = 0 and 0.06 samples when T is normalized by T_c. This finding implies that in these two samples, the SC gap $\Delta(T)$ is scaled by T_c, despite the suppression of T_c for y = 0.06. Hence the Sb-doping effects on the SC gap and T_c for y = 0.06 can mainly be explained not by the pair-breaking effects but by the enhancement of electron correlation due to weak carrier localization. For ensure of that, we used the expression $\frac{C_{es}}{T} - \gamma_0 = \frac{(\gamma_N - \gamma_0)T_C a}{T} \exp\left(-\frac{\Delta(0)}{k_B T}\right)$ of the fully gapped BCS result to fit the data of the electronic specific heat at low temperatures below $T << T_c$ for y = 0 and 0.06, as shown in Fig. 4.11. We obtained the size of the gap $\Delta(0) = 1.0 k_B T_c$ over the low-temperature range ($T < 0.3T_c$) in both two samples. The impurity effect for $LaO_{0.5}F_{0.5}Bi_{1-y}Sb_yS_2$ (y = 0.06) indicates an s-wave gap that is consistent with the result of the pure sample under the condition of microdoping, despite the suppression of T_c.

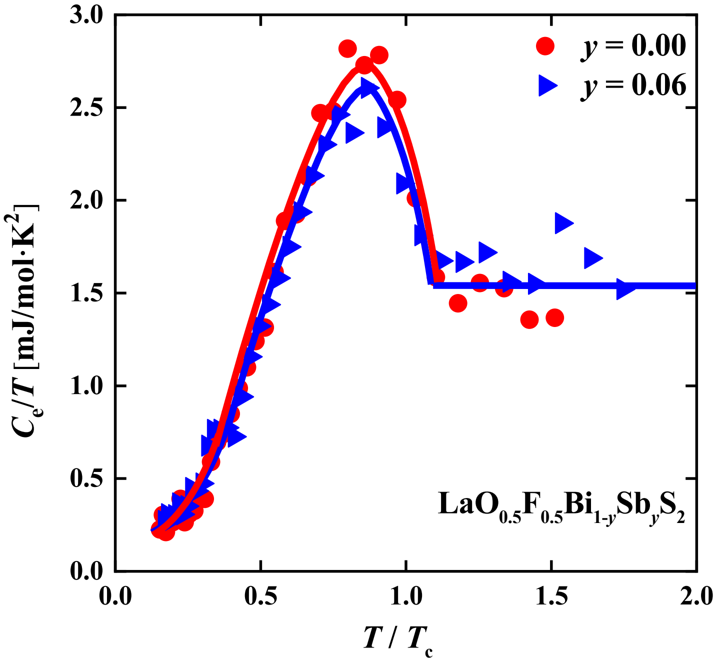

Fig. 4.10 C_e/T vs T/T_c of $LaO_{0.5}F_{0.5}Bi_{1-y}Sb_yS_2$.

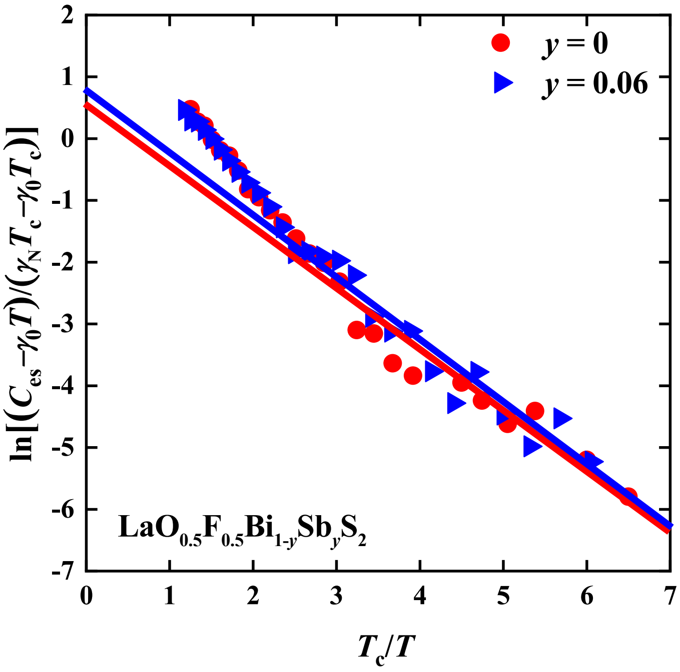

Fig. 4.11 Exponential type of electronic specific heat of $LaO_{0.5}F_{0.5}Bi_{1-y}Sb_yS_2$. Solid line represents the linear fit of the data.

4.6 Discussions and conclusions of $LaO_{0.5}F_{0.5}Bi_{1-y}Sb_yS_2$ (y = 0–0.2)

Assuming a single anisotropic gap, the C_e for Sb-free and Sb-doped samples has small but finite γ_0-value. The finite γ_0-value may seem to be caused by pair-breaking effects in a nodal superconductor with impurities, which can explain the large anisotropy of SC gap reported in ARPES experiments. [59] However, we used the theoretical results of Ichikawa group [60] about impurity effects in BiS_2-based layered superconductors to compare with our results. In Ichikawa groups results, the nodal extended s-wave gap symmetry was supposed as shown in Fig. 4.12 and Fig. 4.13. Based the results of Ichikawa group, $\zeta = \frac{\alpha}{2\pi T_{c0}}$ and $\xi = \frac{\alpha}{\Delta}$ are defined, where α is a pair-breaking parameter proportional to impurity concentration and T_{c0} is the superconducting transition temperature without non-magnetic impurity. Figure 4.12 shows T_c/T_{c0} versus ζ for the nodal extended s-wave gap with p = 0, 0.5, 1.0, and 1.5, where p is ratio of isotropic to anisotropic gaps. Their results indicate that transition temperature is suppressed with increasing impurity scattering, and it is consistent with our results. Furthermore, there is small but finite γ_0-value when p = 0 and 0.5 as shown in Fig. 4.13. So, γ_0 versus ξ with p = 0 and 0.5 are summarized in Fig. 4.14. Their results indicate that γ_0-value is increasing with increasing impurity scattering for the nodal extended s-wave gap, but in our study, γ_0-value and SC gap $\Delta(T)$ are hardly affected by Sb-doping despite the suppression of T_c. It is well known that non-magnetic impurities do not affect the density of states at the Fermi level in s-wave conventional superconductors. Above all, the results of C_e in Sb-doped samples will rule out the existence of nodes in the SC gap, and the symmetry of SC gap is suggested to be *s*-wave with full gap.

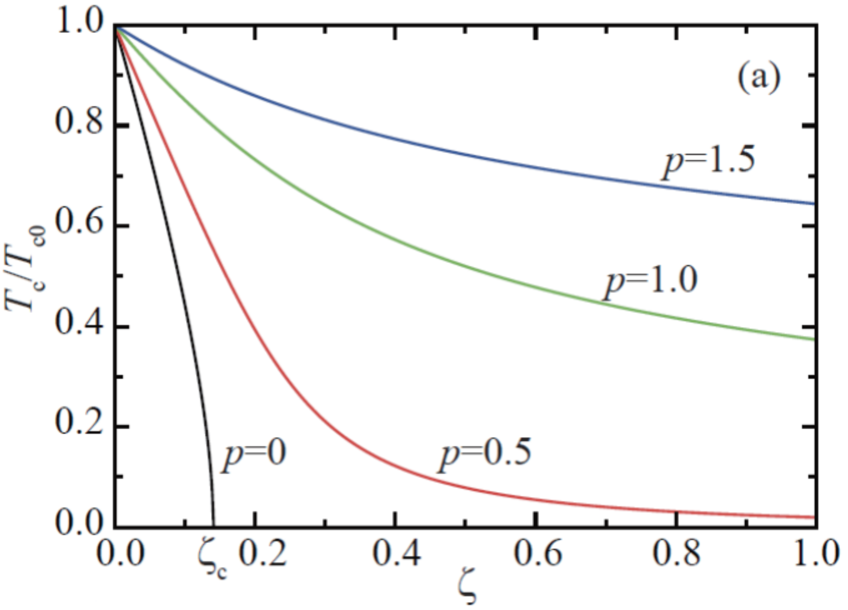

Fig. 4.12 T_c/T_{c0} vs ζ for the nodal extended *s*-wave gap with p = 0, 0.5, 1.0, and 1.5.

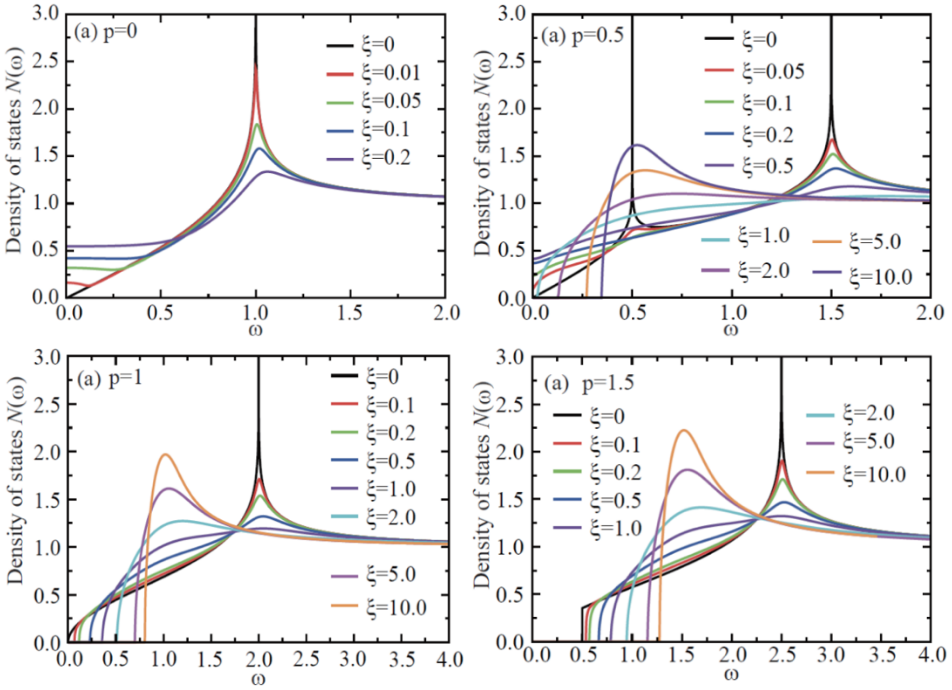

Fig. 4.13. Density of state vs frequency for the nodal extended *s*-wave gap with p = 0, 0.5, 1.0, and 1.5.

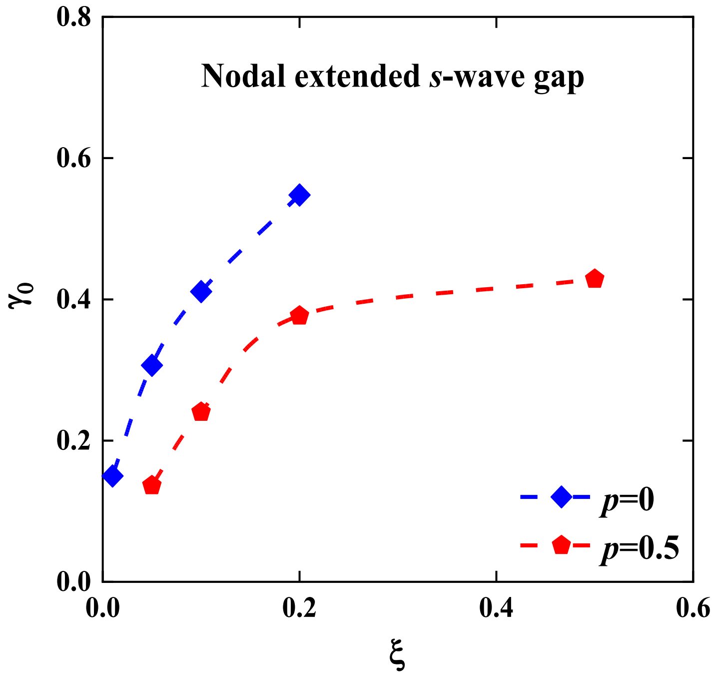

Fig. 4.14 γ_0 vs ξ for the nodal extended *s*-wave gap with p = 0 and 0.5.

In $LaO_{0.5}F_{0.5}Bi_{1-y}Sb_yS_2$, T_c is suppressed by the Sb-doping in both the specific heat and the electrical resistivity and magnetic susceptibility measurements. The slight decrease in T_c in Sb-doped samples can be ascribed to the enhancement of electron correlations due to the weak localization of carriers. However, γ_0 proportional to the density of states at the Fermi level in the SC state is hardly recovered below $y = 0.06$. The C_e/T versus T curves for $y = 0$ and 0.06 are scaled with each other by T_c. The SC gap $\Delta(T) = 1.0k_BT_c$ over the low-temperature range ($T < 0.3T_c$) for $y = 0$ and 0.06, despite the suppression of T_c for $y = 0.06$. The T-dependence of C_e/T is very similar between y

= 0 and 0.06, meaning that the Sb-doping of $y = 0.06$ has little effect on the gap structure. These results indicate that the superconductivity in the present system is robust against the pair-breaking due to non-magnetic impurities, as expected in the fully gapped *s*-wave superconductivity without nodes.

Chapter 5

Conclusions

In conclusion, we have synthesized single-crystal samples of $LaO_{1-x}F_xBiS_2$ (x = 0.5, 0.4) and $LaO_{0.5}F_{0.5}Bi_{1-y}Sb_yS_2$ (y = 0–0.20) using the flux method under ambient pressure. From single-crystal X-ray diffraction experiments at room temperature (~290 K), all of samples in the present study show tetragonal symmetry with the $P4/nmm$ space group. The lattice parameters a and c have not changed much in $LaO_{1-x}F_xBiS_2$ (x = 0.5, 0.4) and $LaO_{0.5}F_{0.5}Bi_{1-y}Sb_yS_2$ (y = 0–0.20). These results indicate that the in-plane chemical pressure is positive but very weak in these compounds and that impurity scattering plays an essential role in tuning the electronic state in these compounds.

For $LaO_{1-x}F_xBiS_2$ (x = 0.5, 0.4) superconductors, Meissner diamagnetism was exhibited near T_c in both two samples. The results of T- and H-dependence of the electronic specific heat below T_c indicate that $LaO_{1-x}F_xBiS_2$ (x = 0.5) is a fully gapped superconductor. The SC gap structure has two possibilities; one is an anisotropic single gap, and the other is two gaps with different magnitudes. The results also indicate that $LaO_{1-x}F_xBiS_2$ (x = 0.4) shows bulk superconductivity in a manner similar to $LaO_{1-x}F_xBiS_2$ (x = 0.5), although T_c is slightly suppressed and has a broad transition. From the α-model fitting results, the two-gap effect is more dominant for x = 0.4.

For $LaO_{0.5}F_{0.5}Bi_{1-y}Sb_yS_2$ (y = 0–0.20) superconductors, T_c is suppressed by the Sb-doping in both the specific heat and the electrical resistivity and magnetic susceptibility measurements. Hence the Sb-doping effects on T_c can mainly be explained not by the pair-breaking effects but by the enhancement of electron correlation due to weak carrier localization. However, the SC gap $\Delta(T)$ for y = 0 and 0.06 are scaled with each other by

T_c. The impurity effect for $LaO_{0.5}F_{0.5}Bi_{1-y}Sb_yS_2$ (y = 0.06) indicates an *s*-wave gap that is consistent with the result of the pure sample under the condition of microdoping. γ_0 proportional to the density of states at the Fermi level in the SC state is hardly recovered below y = 0.06. The robustness of the SC gap against the pair-breaking due to non-magnetic impurities means that the SC gap is consistent with a full gap with an *s*-wave symmetry without nodes.

References

[1] H. K. Onnes, Leiden Comm. **124**, 1226 (1911).

[2] W. Meissner, and R. Oschenfeld, Naturwissenschaften **21**, 787 (1933).

[3] F. London, and H. London, Proc. Roy. Soc. **A 149**, 71 (1935).

[4] V. L. Ginzburg, and L. D. Landau, Sov. Phys. JETP **20**, 1064 (1950).

[5] J. Bardeen, L. N. Cooper, and J. R. Schreiffer, Phys. Rev. **108**, 1175 (1957).

[6] J. Bardeen, L. N. Cooper, and J. R. Shrieffer, Phys. Rev. **106**, 162 (1957).

[7] B. D. Josephson, Phys. Lett. **1**, 251 (1962).

[8] G. Bednorz, and K. A. Műller, Z. Phys. B **64**, 189 (1986).

[9] M. K. Wu, J. R. Ashburn, C. J. Torng, P. H. Hor, R. L. Meng, L. Gao, Z. J. Huang, Y. Q. Wang, and C. W. Chu, Phys. Rev. Lett. **58**, 908 (1987).

[10] H. Maeda, Y. Tanaka, M. Fukutomi, and T. Asano, Jpn. J. Appl. Phys. **27**, L209 (1988).

[11] J. Nagamatsu, N. Nakagawa, T. Muranaka, Y. Zenitani, and J. Akimtsu, Nature **410**, 63 (2001).

[12] Y. Kamihara, H. Hiramatsu, M. Hirano, R. Kawamura, H. Yanagi, T. Kamiya, and H. Hosono, J. Am. Chem. Soc. **128**, 10021 (2006).

[13] Y. Kamihara, T. Watanabe, M. Hirano, and H. Hosono, J. Am. Chem. Soc. **130**, 3296 (2008).

[14] Y. Mizuguchi, H. Fujihisa, Y. Gotoh, K. Suzuki, H. Usui, K. Kuroki, S. Demura, Y. Takano, H. Izawa, and O. Miura, Phys. Rev. B **86**, 220510 (2012).

[15] L. R. Testardi, J. H. Wernick, and W. A. Royer, Solid State Comm. **15**, 1 (1974).

[16] A. Junod, J. L. Staudenmann, J. Muller, and P. Spitzli, J. Low Temp. Physics **5**, 25 (1971).

[17] B. T. Matthias, T. H. Geballe, S. Geller, and E. Corenzwit, Phys. Rev. **95**, 1435 (1954).

[18] G. F. Hardy, and J. K. Hulm, Phys. Rev. **93**, 1004 (1954).

[19] S. N. Putillin, E. V. Antipov, O. Chmaissem, and M. Marezio, Nature **362**, 226 (1993).

[20] A. Schilling, M. Cantoni, J. D. Guo, and H. R. Ott, Nature **363**, 56 (1993).

[21] T. Kaneko, Y. Yamauchi, and S.Tanaka, Physica C **178**, 377 (1991).

[22] S. Matsuishi, T. Hanna, Y. Muraba, S. W. Kim, J. E. Kim, M. Takata, S. Shamoto, R. I. Smith, and H. Hosono, Phys. Rev. B **85**, 014514 (2012).

[23] R. Z. An, L. Wei, Y. Jie, Y. Wei, S. X. Li, L. Z. Cai, C. G. Can, D. X. Li, S.L. Ling, Z. Fang, and Z. Z. Xian, Chin. Phys. Lett. **25**, 2215 (2008).

[24] S. He, J. He, W. Zhang, L. Zhao, D. Liu, X. Liu, D. Mou, Y. Ou, Q. Wang, Z. Li, L. Wang, Y. Peng, Y. Liu, C. Chen, L. Yu, G. Liu, X. Dong, J. Zhang, C. Chen, Z. Xu, X. Chen, X. Ma, Q. Xue, and X. J. Zhou, Nat. Mater. **12**, 605 (2013).

[25] N. Spyrison, M. A. Tanatar, K. Cho, Y. Song, P. Dai, C. Zhang, and R. Prozorov, Phys. Rev. B **86**, 144528 (2012).

[26] S. Kitagawa, H. Kotegawa, H. Tou, H. Ishii, K. Kudo, M. Nohara, and H.

Harima, J. Phys. Soc. Jpn. **82**, 113704 (2013).

[27] J. Guo, Y. Qi, S. Matsuishi, and H. Hosono, J. Am. Chem. Soc. **134**, 20001 (2012).

[28] S. Pyon, K. Kudo, and M. Nohara, J. Phys. Soc. Jpn. **81**, 053701 (2012).

[29] Y. Mizuguchi, S. Demura, K. Deguchi, Y. Takano, H. Fujihisa, Y. Gotoh, H. Izawa, and O. Miura, J. Phys. Soc. Jpn. **81**, 114725 (2012).

[30] G. K. Selvan, G. Thakur, K. Manikandan, A. Banerjee, Z. Haque, L. C. Gupta, A. Ganguli, and S. Arumugam, J. Phys. D **49**, 275002 (2016).

[31] D. Yazici, K. Huang, B. D. White, A. H. Chang, A. J. Friedman, and M. B. Maple, Philos. Mag. **93**, 673 (2013).

[32] C. T. Wolowiec, B. D. White, I. Jeon, D. Yazici, K. Huang, and M. B. Maple, J. Phys.: Condens. Matter **25**, 422201 (2013).

[33] C. T. Wolowiec, D. Yazici, B. D. White, K. Huang, and M. B. Maple, Phys. Rev. B **88**, 064503 (2013).

[34] M. Fujioka, M. Nagao, S. J. Denholme, M. Tanaka, H. Takeya, T. Yamaguchi, and Y. Takano, Appl. Phys. Lett. **105**, 052601 (2014).

[35] M. Fujioka, M. Tanaka, S. J. Denholme, T. Yamaki, H. Takeya, T. Yamaguchi, and Y. Takano, Europhys. Lett. **108**, 47007 (2014).

[36] M. Tanaka, T. Yamaki, Y. Matsushita, M. Fujioka, S. J. Denholme, T. Yamaguchi, H. Takeya, and Y. Takano, Appl. Phys. Lett. **106**, 112601 (2015).

[37] Y. Mizuguchi, J. Phys. Soc. Jpn. **88**, 041001 (2019).

[38] T. Yildirim, Phys. Rev. B **87**, 020506 (2013).

[39] Y. Mizuguchi, E. Paris, T. Sugimoto, A. Iadecola, J. Kajitani, O. Miura, T. Mizokawa, and N. L. Saini, Phys. Chem. Chem. Phys. **17**, 22090 (2015).

[40] A. Athauda, J. Yang, S. Lee, Y. Mizuguchi, K. Deguchi, Y. Takano, O. Miura, and D. Louca, Phys. Rev. B **91**, 144112 (2015).

[41] Y. Mizuguchi, T. Hiroi, J. Kajitani, H. Takatsu, H. Kadowaki, and O. Miura, J. Phys. Soc. Jpn. **83**, 053704 (2014).

[42] Y. Mizuguchi, A. Miura, J. Kajitani, T. Hiroi, O. Miura, K. Tadanaga, N. Kumada, E. Magome, C. Moriyoshi, and Y. Kuroiwa, Sci. Rep. **5**, 14968 (2015).

[43] N. Kase, J. Phys. Soc. Jpn. **88**, 041007 (2019).

[44] F. Giubileo, F. Romeo, A. Di Bartolomeo, Y. Mizuguchi, and P. Romano, J. Phys. Chem. Solids. **118**, 192 (2018).

[45] H. Usui, K. Suzuki, and K. Kuroki, Phys. Rev. B **86**, 220501(R) (2012).

[46] T. Agatsuma, and T. Hotta, J. Magn. Magn. Mater. **400**, 73 (2016).

[47] X. Wan, H. C. Ding, S. Y. Savrasov, and C. G. Duan, Phys. Rev. B **87**, 115124 (2013).

[48] Y. Liang, X. Wu, W. F. Tsai, and J. Hu, Front. Phys. **9**, 194 (2014).

[49] Y. Yang, W. S. Wang, Y. Y. Xiang, Z. Z. Li, and Q. H. Wang, Phys. Rev. B **88**, 094519 (2013).

[50] G. B. Martins, A. Moreo, and E. Dagotto, Phys. Rev. B **87**, 081102(R) (2013).

[51] X. Wu, J. Yuan, Y. Liang, and H. Fan, J. Hu: EPL **108** 27006 (2014).

[52] Shruti, P. Srivastava, and S. Patnaik, J. Phys.: Condens. Matter **25**, 312202 (2013).

[53] G. Lamura, T. Shiroka, P. Bonfa, S. Sanna, R. De Renzi, C. Baines, H. Luetkens, J. Kajitani, Y. Mizuguchi, O. Miura, K. Deguchi, S. Demura, Y. Takano, and M. Putti, Phys. Rev. B **88**, 180509(R) (2013).

[54] L. Jiao, Z. F. Weng, J. Z. Liu, J. L. Zhang, G. M. Pang, C. Y. Guo, F. Gao, X. Y. Zhu, H. H. Wen, and H. Q. Yuan, J. Phys.: Condens. Matter **27**, 225701 (2015).

[55] T. Yamashita, Y. Tokiwa, D. Terazawa, M. Nagao, S. Watauchi, I. Tanaka, T. Terashima, and Y. Matsuda, J. Phys. Soc. Jpn. **85**, 073707 (2016).

[56] N. Kase, Y. Terui, T. Nakano, and N. Takeda, Phys. Rev. B **96**, 214506 (2017).

[57] K. Hoshi, Y. Goto, and Y. Mizuguchi, Phys. Rev. B **97**, 094509 (2018).

[58] J. Zhang, K. Huang, Z. F. Ding, D. E. MacLaughlin, O. O. Bernal, P. C. Ho, C. Tan, X. Liu, D. Yazici, M. B. Maple, and L. Shu, Phys. Rev. B **94**, 224502 (2016).

[59] Y. Ota, K. Okazaki, H. Q. Yamamoto, T. Yamamoto, S. Watanabe, C. Chen, M. Nagao, S. Watauchi, I. Tanaka, Y. Takano, and S. Shin, Phys. Rev. Lett. **118**, 167002 (2017).

[60] A. Ichikawa, and T. Hotta, J. Phys. Soc. Jpn. **87**, 114706 (2018).

[61] Y. Mizuguchi, J. Phys. Chem. Solids. **84**, 34 (2015).

[62] S. Maekawa and H. Fukuyama, J. Phys. Soc. Jpn. **51**, 1380 (1982).

[63] F. Bouquet, Y. Wang, R. A. Fisher, D. G. Hinks, J. D. Jorgensen, A. Junod, and N. E. Phillips, Europhys. Lett. **56**, 856 (2001).

Publications

[1] Sho Iwasaki, Yoshiki Kawai, Shotaro Takahashi, Takaya Suda, **Ying Wang**, Yasunori Koshino, Fumiya Ogura, Yoshiyuki Shibayama, Tohru Kurosawa, Migaku Oda, Masayuki Ido, and Naoki Momono, Journal of the Physical Society of Japan Vol 88. No.4. P041005-1—041005-10.

[2] **Ying Wang**, Shotaro Takahashi, Takaya Suda, Taro Tamura, Haruka Ohta, Tohru Kurosawa, Migaku Oda, Masayuki Ido, Naoki Momono, Journal of the Physical Society of Japan Vol 89. No.9. P094708-1—094708-6.

Presentations

[1] Impurity effects on the superconductivity in $LaO_xF_{1-x}BiS_2$

73rd Annual Meeting, The Physical Society of Japan, Tokyo, 22aPs-21 2018.03.22

[2] Impurity effects on the superconductivity in $LaO_{0.5}F_{0.5}BiS_2$

12th International Conference on Materials and Mechanisms of Superconductivity and High Temperature Superconductors, Beijing, Tu-86 2018.08.21

[3] The Electronic Specific heat in the Superconducting State of a Bismuth Sulfide Superconductor

The 4th Emallia Conference 2018, Sapporo, Talk No.17 2018.07.24

[4] Impurity Effects on the Superconductivity in $LaO_{0.5}F_{0.5}BiS_2$

Spectroscopies in Novel Superconductors 2019, Tokyo, Tu-28 2019.06.18

[5] Impurity Effects on the Superconductivity in $LaO_{0.5}F_{0.5}BiS_2$

Muroran-IT Rare Earth Workshop 2018, Toya, PO-14 2018.11.8

Acknowledgements

First, I would like to express my deepest gratitude to my supervisor professor Naoki Momono for his constant encouragement and instructive advice on my research and daily life. He gave me the valuable opportunity to come to Japan and opened my horizon in the academic studies. He helped me a lot in life and study. He also walked me through all the stages of the writing of this thesis.

I would like to express my heartfelt gratitude to professor Takano Hideaki in Radiation Properties Laboratory and professor Ebisu Shuji in Low Temperature Properties Laboratory for their help and suggestions given to me during my study.

I would like to thank the staffs in the center for international relations, my Japanese was poor, they kindly help me many things in life.

I would also like to thank all my friends and my laboratory staffs for all kinds of helps during my study in Muroran Institute of Technology.

Last, I would like to thank my husband and my parents for their spiritual support during my study in Japan.

2020.9

WANG YING